University of North Dakota
UND Scholarly Commons

Theses and Dissertations | Theses, Dissertations, and Senior Projects

2015

Interplay of porous media and fracture stimulation in sedimentary enhanced geothermal systems : Red River Formation, Williston Basin, North Dakota

Caitlyn M. Hartig
University of North Dakota

Follow this and additional works at: https://commons.und.edu/theses

 Part of the Geology Commons

Recommended Citation

Hartig, Caitlyn M., "Interplay of porous media and fracture stimulation in sedimentary enhanced geothermal systems : Red River Formation, Williston Basin, North Dakota" (2015). *Theses and Dissertations*. 128.
https://commons.und.edu/theses/128

This Thesis is brought to you for free and open access by the Theses, Dissertations, and Senior Projects at UND Scholarly Commons. It has been accepted for inclusion in Theses and Dissertations by an authorized administrator of UND Scholarly Commons. For more information, please contact zeineb.yousif@library.und.edu.

INTERPLAY OF POROUS MEDIA AND FRACTURE STIMULATION IN SEDIMENTARY ENHANCED GEOTHERMAL SYSTEMS: RED RIVER FORMATION, WILLISTON BASIN, NORTH DAKOTA

by

Caitlin M. Hartig
Bachelor of Science, Pennsylvania State University, 2013
Bachelor of Musical Arts, Pennsylvania State University, 2013
Geographic Information Systems (GIS) Certificate, University of North Dakota, 2014

A Thesis

Submitted to the Graduate Faculty

of the

University of North Dakota

in partial fulfillment of the requirements

for the degree of

Master of Science

Grand Forks, North Dakota

May

2015

This thesis, submitted by Caitlin M. Hartig in partial fulfillment of the requirements for the Degree of Master of Science from the University of North Dakota, has been read by the Faculty Advisory Committee under whom the work has been done and is hereby approved.

WD Gosnold
William D. Gosnold

Hadi Jabbari

Richard LeFever

This thesis is being submitted by the appointed advisory committee as having met all of the requirements of the School of Graduate Studies at the University of North Dakota and is hereby approved.

Wayne Swisher
Dean of the School of Graduate Studies

April 29, 2015
Date

PERMISSION

Title Interplay of Porous Media and Fracture Stimulation in Sedimentary Enhanced Geothermal Systems: Red River Formation, Williston Basin, North Dakota

Department Geology

Degree Master of Science

In presenting this thesis in partial fulfillment of the requirements for a graduate degree from the University of North Dakota, I agree that the library of this University shall make it freely available for inspection. I further agree that permission for extensive copying for scholarly purposes may be granted by the professor who supervised my thesis work or, in his absence, by the Chairperson of the department or the dean of the School of Graduate Studies. It is understood that any copying or publication or other use of this thesis or part thereof for financial gain shall not be allowed without my written permission. It is also understood that due recognition shall be given to me and to the University of North Dakota in any scholarly use which may be made of any material in my thesis.

Caitlin M. Hartig
4 May 2015

TABLE OF CONTENTS

LIST OF FIGURES

Figure Page

LIST OF TABLES

ACKNOWLEDGEMENTS

First and foremost, I would like to sincerely thank all members of my advisory committee for their instruction and guidance with this project. I express my heartfelt gratitude to Dr. William Gosnold, Dr. Hadi Jabbari, and Dr. Richard LeFever for all of their assistance.

I am indebted to Fred Anderson and Elroy Kadrmas for their GIS shapefile of digitized surface lineaments over the Williston 250k in North Dakota. Without this file, my geostatistical analysis of the natural fracture orientation would have been infeasible.

Furthermore, I would like to express my gratitude to my GIS professors for all of their invaluable advice. I am grateful to Dr. Gregory Vandeberg, Dr. Michael Niedzielski, and Dr. Enru Wang for all of their assistance.

I would like to sincerely thank Anna Crowell, Faye Ricker, Josh Crowell, Bailey Bubach, and Dylan Young-- my colleagues on the UND geothermal team-- for assisting me with various aspects of this project. Furthermore, I am grateful to Grant Ferguson, Jacek Scibek, Jamie Russell, and Earl Klug for their ideas and source material.

Moreover, I would like to extend a huge thank you to my friends for all of their moral support. Charis Dalessio, Haijing Chen, Amber Sharkawy, and Lisa Huber, I could not have done it without you.

Last but not least, thank you to my favorite Starbucks crew on 32nd Avenue South. You guys are seriously the best.

ABSTRACT

Fracture stimulated enhanced geothermal systems (EGS) can be installed in both crystalline rocks and sedimentary basins. The Red River Formation (Ordovician), which lies between 3.6 and 4.2 km depth in the Williston Basin, is a viable site for installation of sedimentary EGS (SEGS). SEGS is possible there because temperatures in the formation surpass 140° Celsius and the permeability is 0.1-38 mD; fracture stimulation can be utilized to improve performance. The main objectives of this project were 1) to determine the spatial variation of the intrinsic properties of the Red River Formation across the study area, and 2) to understand the natural fracture orientation/location in the subsurface of the study area. Maps of the intrinsic properties of the Red River Formation-- including depth to the top of the formation, depth to the bottom of the formation, porosity, heat flow, geothermal gradient, and temperature-- were produced by the Kriging interpolation method in ArcGIS. A GIS and geostatistical analysis was completed to show that there is a satisfactory correlative relationship between the surface lineaments and the basement faults in the study area. Consequently, the orientations and locations of the surface lineaments and basement faults were combined in a shapefile to represent the area's discrete fracture network. In the future, the results of these two analyses can be utilized to create a reservoir simulation model of an SEGS in the Red River Formation; the purpose of this model would be to ascertain the thermal response of the reservoir to fracture stimulation.

CHAPTER I

INTRODUCTION TO THE RESEARCH PROBLEM

Executive Summary

Fracture stimulated enhanced geothermal systems (EGS) can be installed in both crystalline rocks and sedimentary basins. The Red River Formation (Ordovician), which lies between 3.6 and 4.2 km depth in the Williston Basin, is a viable site for installation of sedimentary EGS (SEGS). SEGS is possible there because temperatures in the formation surpass 140° Celsius and the permeability is 0.1-38 mD; fracture stimulation can be utilized to improve performance. The main objectives of this project were 1) to determine the spatial variation the Red River Formation intrinsic properties across the study area, and 2) to understand the natural fracture orientation/location in the subsurface of the study area.

Background to Geothermal and SEGS

The geothermal industry is currently struggling due to the high upfront financial cost of geothermal systems, which limits market viability. The high upfront cost comes from the high risk that is associated with exploration, production, and well drilling of geothermal systems. The high risk comes from a paucity of subsurface information. Consequently, geothermal industry leaders disagree on which techniques are the most economically viable, and therefore where to distribute funds.

While some organizations-- for instance the U.S. Department of Energy-- advocate for fracture stimulated Enhanced Geothermal Systems (EGS) installation in crystalline rocks, other geothermal experts, such as David Blackwell, Paul Morgan, and Tom Anderson,

advocate for EGS in sedimentary basins (Blackwell et al., 2006; Morgan, 2013; Anderson, 2013). Sedimentary reservoirs have an edge over crystalline reservoirs when it comes to EGS because even a small amount of the sedimentary basin's higher intrinsic permeability will increase the efficiency of heat extraction (Tester et al., 2006). Furthermore, SEGS is attractive because it utilizes existing oil field data; because of this, general knowledge of the formation properties is improved and the cost of drilling is accordingly lowered.

In addition to having an edge over crystalline EGS, SEGS has an edge over conventional sedimentary geothermal systems in the deeper formations of the basin. This advantage is due to the fact that the rocks at the base of sedimentary basins (at depths greater than 3 km) are similar in permeability and porosity to those in the basement (Tester et al., 2006), with porosity about 20% and permeability about 25 mD. Therefore, it is actually necessary to hydroshear the lower formations of sedimentary basins in order to improve the permeability there, such that geothermal heat extraction would be feasible.

Moreover, many of the drawbacks that are associated with heat extraction from both crystalline EGS and conventional sedimentary geothermal systems are reduced in an SEGS. The main drawbacks of crystalline EGS include: 1) low permeability between the injection and production wells, 2) difficulty in extracting sufficiently hot temperatures near the Earth's surface, i.e. requires deep drilling, and 3) limited lifespan of the system (Anderson, 2013). The main drawback of sedimentary geothermal systems is that only low temperatures can be extracted from the potential reservoirs (Anderson, 2013). In an SEGS, on the other hand, the rock units have a higher permeability between the injection and production wells, moderate temperatures (~150° C) can be extracted in the upper 4-5 km of the crust, and the system can potentially be sustainable.

There are few SEGS currently on-line. A successful low-to-intermediate-temperature binary unit project was previously successful in Maguarichic, Mexico (Blodgett, 2010) but is no longer functional. In Germany, there are three main SEGS installed: Unterhaching, Landau, and Horstberg. Unterhaching and Landau currently produce electricity with cascaded heat, and Landau and Horstberg have demonstrated success with use of hydraulic fracturing on low permeability sedimentary rocks (Morgan, 2013).

In the United States, an SEGS went on-line in Desert Peak, Nevada, in 2013. The SEGS has already proven to be successful with its 175-fold increase in injectivity in the target formation, use of cost-effective techniques and technologies, and effective approach to multi-phase stimulation (Chabora and Zemach, 2013). The addition of fracture stimulation to the Desert Peak reservoir resulted in a 38% increase in productivity ("Geothermal energy Hot rocks," 2014).

Several other SEGS projects have been considered for development in the United States, but so far only Desert Peak has been implemented. Some of the sedimentary basins that are candidates for SEGS installation include the Anadarko, Bighorn, Denver, East Texas, Ft. Worth, Green River, Great Bain, Hannah, Delaware, Northern Louisiana, Powder River, Raton, Sacramento, San Joaquin, Uinta, Williston, and Wind River basins (Porro and Augustine, 2014; Blackwell et al., 2006). Because existing binary plants for moderate temperature (150° C) SEGS have already proven to be successful, SEGS in the Williston Basin within the Red River Formation, where temperatures are comparable, should be viable.

Research Area

As a result of its prominent geothermal potential and interconnectedness in a discrete fracture network, the Williston Basin was selected as a potential candidate for SEGS

installation. A 60.0 km by 14.7 km (882 km^2) section of the basin beneath the Nesson Anticline in western North Dakota-- surrounding the junction of Divide, Burke, Williams, and Mountrail counties-- was designated as the specific study area for this project (Figure 1).

In addition to having a large amount of thermal energy in place, the Williston Basin has good reservoir productivity. There is an estimated $3.4*10^{19}$ KJ of thermal energy in place in the Williston Basin, including both the rock and the pore fluids (Porro and Augustine, 2014). In order for a reservoir to be classified as having "great" reservoir productivity, there should be high flow volumes, vertical permeability, strong hydrothermal recharge, and a well-known thermal profile (Porro and Augustine, 2014). Because it meets most of these standards, the Williston Basin has been classified as ranging from "great to good" reservoir productivity (Porro and Augustine, 2014).

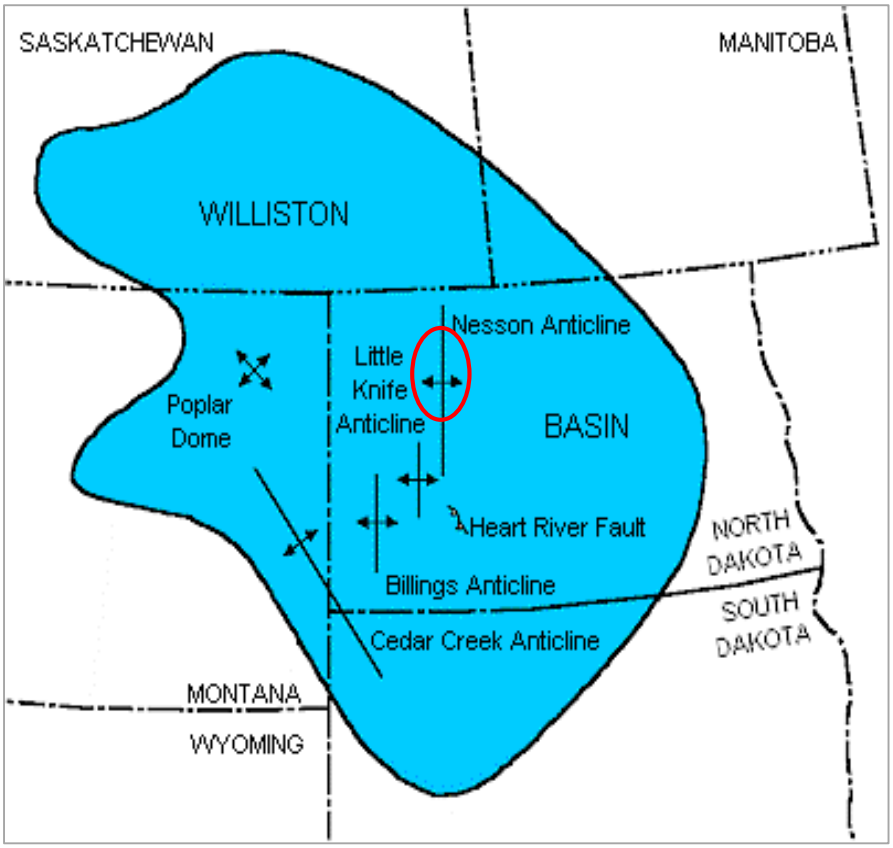

Figure 1: Nesson Anticline Area, Williston Basin (William Gosnold, Pers. Comm., 2013).

The reservoir productivity is greatly improved by the presence of a discrete fracture network in the subsurface. The existing stress field in the Williston Basin is such that natural

stress fractures form from overpressure and interconnect as a result of tight spacing (Freisatz, 1995). This interconnectivity in the subsurface facilitates geothermal heat extraction because there is a medium of travel available for the injected SEGS fluids.

Research Site

The Red River Formation (Ordovician) has been identified as a potential target for installation of SEGS in the Williston Basin as a result of its oil production history, intrinsic rock properties, and temperature. Because Red River Units B and C have been tapped for oil production, there is sufficient data and information available about the formation on the North Dakota Oil and Gas Division website (https://www.dmr.nd.gov/oilgas/) that can be utilized for analysis.

Furthermore, the Red River Formation has porosity and permeability that are conducive for SEGS installation because the lithology consists mostly of limestones and dolostones (Tanguay and Friedman, 2001). The limestones are mainly composed of calcite and contain minor amounts of dolostone, anhydrite, quartz, and halite (Tanguay and Friedman, 2001). The dolostones are mainly composed of dolomite and calcite and contain traces of quartz, anhydrite, and halite (Tanguay and Friedman, 2001). While the porosity and permeability are “very low to low” in the limestones, porosity and permeability are “low to moderate” in the dolostones (porosity of 10-24% and permeability of <1-62.8 mD, respectively) (Tanguay and Friedman, 2001). Because the porosity and permeability are low to moderate, the Red River Formation is a candidate for SEGS installation.

The temperature of the Red River Formation was initially determined from bottom-hole temperature (BHT) data from the North Dakota Oil and Gas Division Website. These BHT were measured from an instrument that recorded the temperature directly at the bottom

of the wellbore (Richard LeFever, Pers. Comm., 2015). Because BHTs are seldom measured when the wellbore is at thermal equilibrium with the surrounding rock mass, it is necessary to correct the temperatures to improve the accuracy of the measurements (Blackwell and Richards, 2004a; Crowell and Gosnold, 2011; Crowell et al., 2011).

In spite of this, BHT measurements are still fairly unreliable predictors of subsurface temperature after correction, Figures 2-4 (William Gosnold, Pers. Comm., 2015) show that even corrected BHTs do not follow the standard temperature/depth profile for the earth's crust as predicted from the constant heat flow and depth of the stratigraphy for the NDGS wellbores (obtained from the North Dakota Oil and Gas Division website). Corrected temperatures still tend to underestimate the temperatures, particularly for depths greater than 2.5 km.

Because of the erratic nature of BHT measurements, a second method was subsequently utilized to refine the corrected BHTs of the Red River Formation to improve

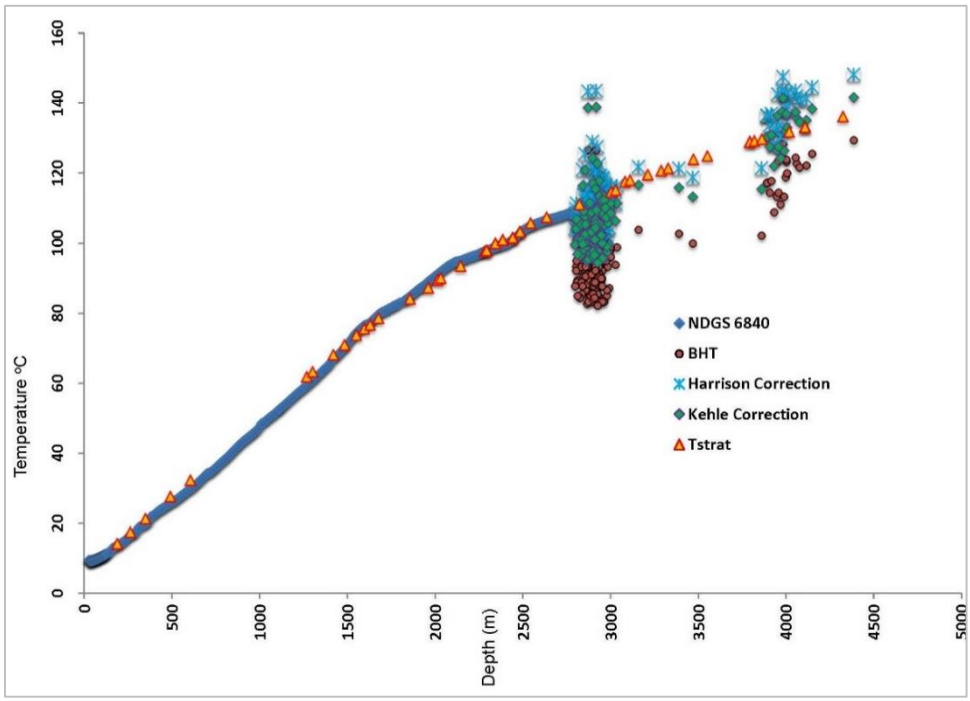

Figure 2: TSTRAT Plot for NDGS 5086 (William Gosnold, Pers. Comm., 2015).

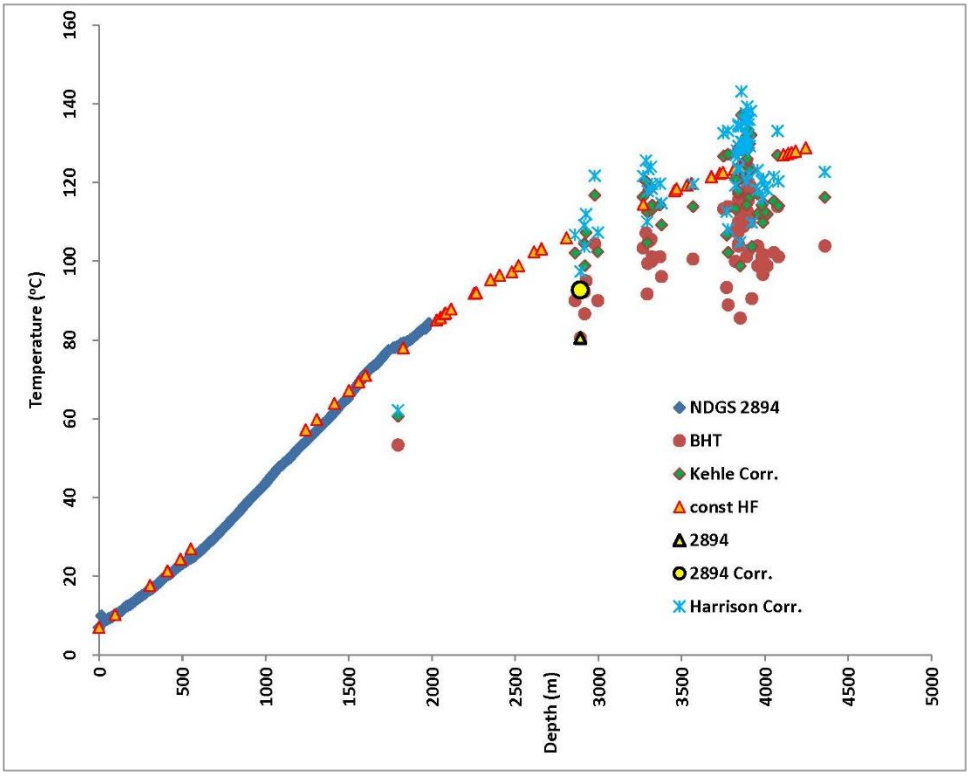

Figure 3: TSTRAT Plot for NDGS 6840 (William Gosnold, Pers. Comm., 2015).

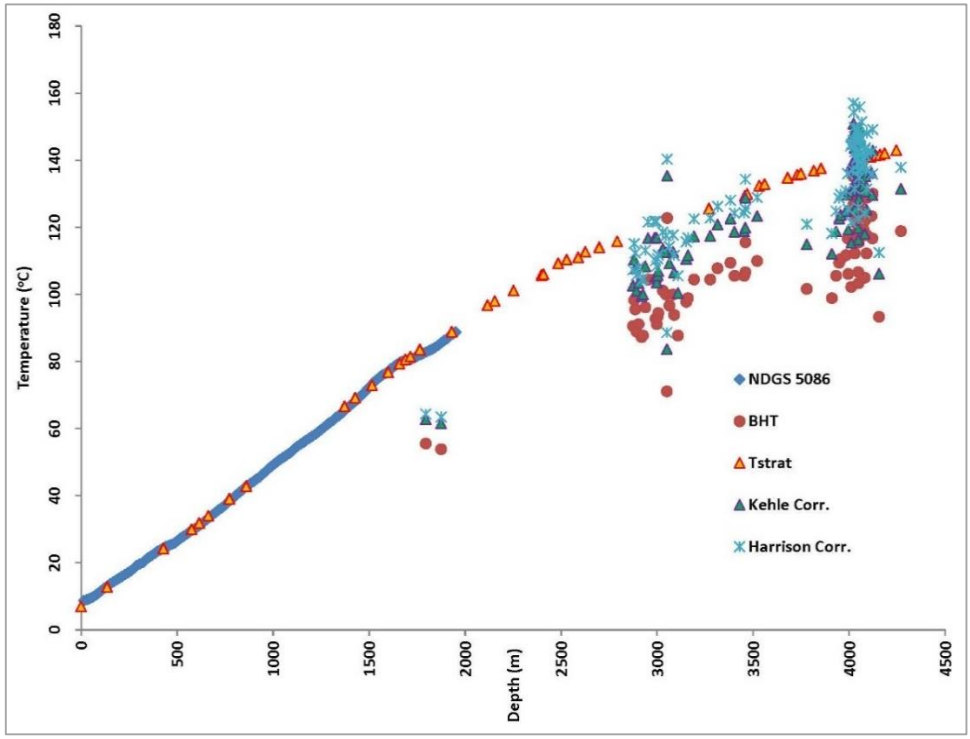

Figure 4: TSTRAT Plot for NDGS 2984 (William Gosnold, Pers. Comm., 2015).

the accuracy of the measurements. This method for obtaining formation temperatures has been applied in previous regional and detailed assessments of geothermal resources in sedimentary basins (Gosnold, 1984; Gosnold, 1991; Gosnold, 1999; Gosnold et al., 2010; Crowell and Gosnold, 2011; Crowell et al., 2011; Gosnold et al., 2012) and in the Geothermal Map of North America (Blackwell and Richards, 2004b). The assumptions of this method are that 1) heat flow is conductive and constant, and 2) the geothermal gradient varies inversely with thermal conductivity according to Fourier's Law:

$$q = \frac{dT}{dz}\lambda \tag{1}$$

where q is heat flow (mW/m^2), $\frac{dT}{dz}$ is the geothermal gradient (°C/m), and λ is thermal conductivity (W/mK). Using this method, Red River Formation BHTs were input as geothermal gradients into Equation 1 in order to obtain the heat flow. Once the heat flow had been obtained for each well, the results were then input into Equation 2 in order to calculate the subsurface temperature at each location:

$$T(z) = T_0 + \sum_{i=1}^{n} \frac{qz_i}{\lambda_i} \tag{2}$$

where $T(z)$ is temperature at depth z (°C), T_0 is surface temperature (°C), q is heat flow (mW/m^2), z_i is formation thickness (m) and λ_i is the formation thermal conductivity (W/mK).

Upon examining the Root Mean Square Error (RMSE) of the maps generated for both the corrected temperatures and the calculated temperatures, the RMSE is lower for the map of the calculated temperatures. Consequently, calculation is a more accurate method of temperature prediction than is BHT correction alone. As a result of this analysis, temperatures in the Red River Formation were found to surpass 140° C; therefore, the reservoir temperature is sufficiently high for heat extraction using SEGS.

Economics

It is currently difficult to compare the cost of geothermal heat extraction to the cost oil and gas extraction. Currently, few wells exist that are deeper than 2750 m (Tester et al., 2006). To ameliorate this problem, the MIT Depth Dependent drilling index was developed and used to normalize the predicted and actual completed geothermal well costs prior to 2004, such that they can be compared to oil and gas well costs (Tester et al., 2006).

There are a few differences in well design between geothermal wells and oil and gas wells. Oil and gas wells typically use 6 3/4" or 6 1/4" bits; furthermore, they are lined with 4 1/2" or 5" casing that is almost always cemented in place and then shot perforated. On the other hand, (vertical) geothermal wells are usually completed with 10 3/4" or 8 1/2" bits; they are lined with 9 5/8" or 7" casing that is generally slotted or perforated instead of cemented (Tester et al., 2006). Therefore, most (vertical) geothermal wells are two to five times more expensive than oil and gas wells due to the higher cost of larger completion diameters (Tester et al., 2006). According to Continental Resources, horizontal geothermal wells are typically cheaper than vertical geothermal wells because they are generally smaller, around 4 1/2" (www.contres.com); as a result of this, horizontal geothermal wells may have pricing that is comparable to oil and gas wells.

While oil and gas drilling is generally cheaper than geothermal drilling, the economics within geothermal drilling are significantly better for EGS in sedimentary rocks than for EGS in crystalline rocks due to the differences in rock type and required drilling depth. The hard, abrasive crystalline rocks reduce the rate of drilling penetration as well as bit life, thereby increasing both the need for trips and the nonrotating drilling costs for the project (Tester et al., 2006). On the other hand, these problems are alleviated in softer

sedimentary rocks. Moreover, the depth to the heat source is less in sedimentary basins than it is in crystalline rocks, with the exceptions of the Basin and Range province, the Cascade Range, and the Pacific-North American plate boundary. Therefore, fewer resources are needed to reach the heat source in sedimentary rocks; thus the project completion time will be faster. Given this information, sedimentary EGS is considerably less expensive than crystalline EGS, with an estimated 20% cost savings (Tester et al., 2006)

Furthermore, the drilling cost is influenced by the number of required casing intervals, which increases with depth. For a geothermal well at 5 km depth, a 4-casing well costs $7.0 million to drill, whereas a 5-casing well costs $8.3 million to drill (Tester et al., 2006). For a geothermal well at 4-5 km depth, four or five casing intervals are needed (Tester et al., 2006). Because the Red River Formation is relatively shallow, at 4.0 km depth, it is likely that four casing intervals would be sufficient, thereby reducing the cost.

To sum up, the cost of vertical geothermal drilling is two to five times more expensive than the cost of oil and gas drilling as a result of the larger completion diameters. On the other hand, horizontal geothermal drilling may be more cost comparable. Within geothermal drilling, heat extraction in sedimentary basins has significantly lower costs than heat extraction in crystalline EGS because 1) the softer rocks facilitate drilling, 2) the depth to the heat source is less, and 3) fewer casings are needed to complete the drilling.

Hypothesis

The hypothesis for this research project was that SEGS is feasible in the Red River Formation of the Williston Basin. To test this hypothesis, subsurface temperatures were examined, as well as the mechanism for fluid flow in the subsurface.

Research Objectives

The main objectives of this research project were 1) to determine the spatial variation of the intrinsic properties of the Red River Formation across the study area, and 2) to understand the natural fracture orientation and location in the subsurface of the study area. By completing these two objectives, a reservoir simulation model of the study area can be completed in order to investigate the potential of the Red River Formation as a site for SEGS installation.

Research was completed in the University of North Dakota Geothermal Laboratory in Grand Forks, North Dakota. The advisory committee consisted of Dr. William Gosnold (geothermics, geophysics, and structural geology), Dr. Hadi Jabbari (reservoir engineering and hydraulic fracturing), and Dr. Richard LeFever (sedimentology and stratigraphy).

Deliverables

Maps of the intrinsic properties of the Red River Formation-- including depth to the top of the formation, depth to the bottom of the formation, porosity, heat flow, geothermal gradient, and temperature-- were produced by the Kriging interpolation method in ArcGIS. Furthermore, a GIS and geostatistical analysis was completed to show that there is a satisfactory correlative relationship between the surface lineaments and the basement faults in the study area. Consequently, the orientations and locations of the surface lineaments and basement faults were combined in a shapefile to represent the area's discrete fracture network. In the future, the results of these two analyses can be utilized to create a reservoir simulation model of an SEGS in the Red River Formation; the purpose of this model would be to ascertain the thermal response of the reservoir to fracture stimulation.

CHAPTER II

RED RIVER FORMATION INTRINSIC PROPERTIES

Research Question

In order to determine the spatial variation of the intrinsic properties of the Red River Formation over the study area (Figure 5), interpolations were completed in ArcGIS using well data from the North Dakota Oil and Gas Division website. The following parameters were interpolated: depth to the top of the formation, depth to the bottom of the formation, permeability, porosity, heat flow, geothermal gradient, and temperature.

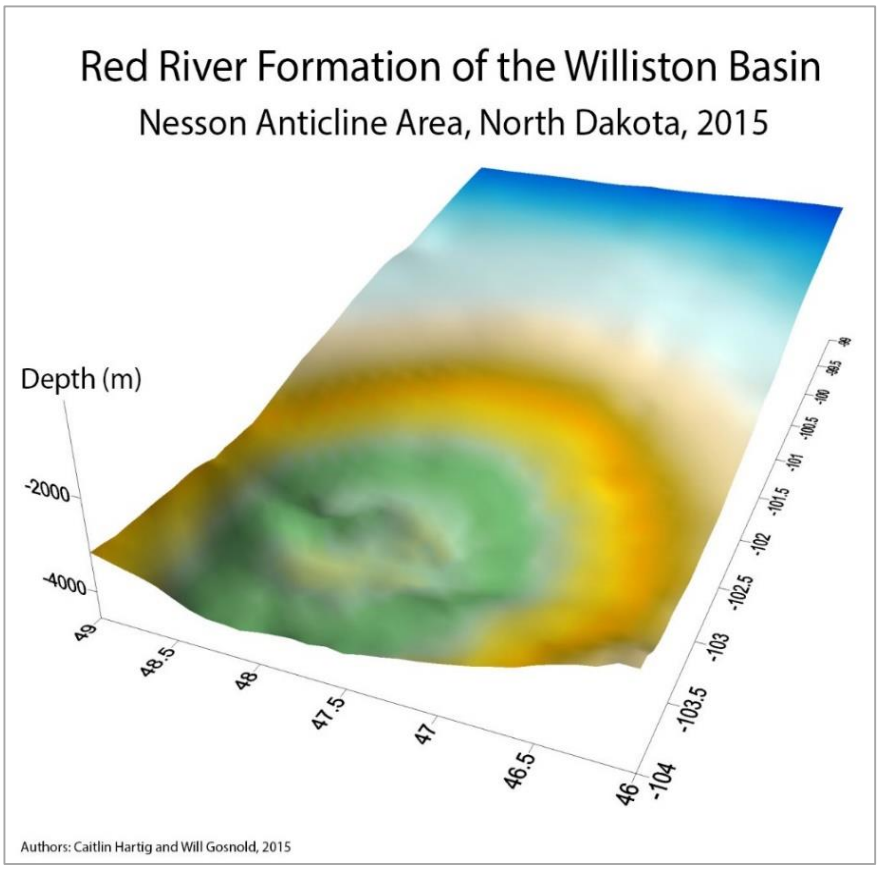

Figure 5: Red River Formation of the Williston Basin. Nesson Anticline Area is shown in green in western North Dakota.

GIS Interpolations

The majority of the interpolations for the Red River Formation were completed using the Kriging method, with the exception of the permeability; the Inverse Distance Weighted (IDW) method was used instead to interpolate the permeability because the data were scarce. The Kriging method of interpolation uses a semivariogram to determine the spatial autocorrelation between points. On the other hand, the IDW method of interpolation uses the inverse of the distance from the sample point to the target location to calculate the interpolated value at the sample point. Regardless of the method used, the interpolations with the lowest Root Mean Square Error (RMSE) were selected as the best models.

For complete accuracy to be obtained using the Kriging method, there need to be 150 or more data points. While there were only 81 total wells in this study area, the Kriging method was utilized anyway-- instead of the IDW method-- because the interpolations had much lower RMSE than they did with the IDW method. While the general error was reduced using the Kriging method, it should be noted that some artifacts were added incorrectly to the Kriging interpolations where there were no wells.

Data for the depth to the top of the formation (81 wells) and depth to the bottom of the formation (36 wells) were obtained from the North Dakota Oil and Gas Division website. The interpolation for the depth to the top of the formation is shown in Figure 6. Initially, the 36 wells were interpolated for the depth to the bottom of the formation with the goal of obtaining the depths for the remaining 45 wells from that map. However, this method failed due to lack of data coverage on the top of the study area. Therefore, to calculate the depth to the bottom of the formation for the remaining 45 wells, the average unit thickness for the Red River Formation was calculated and added to the depth to the top of the formation.

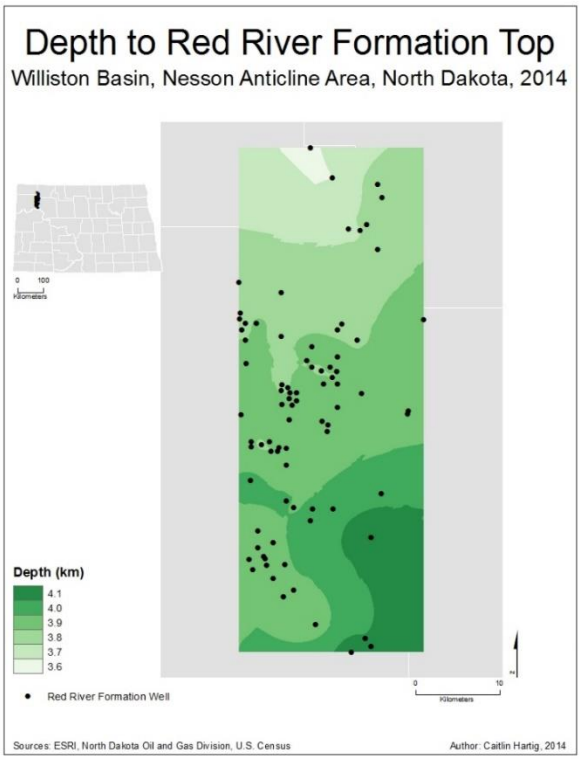

Figure 6: Depth to Red River Formation Top. Interpolation was completed using the Ordinary Kriging method; RMSE = 0.03387275.

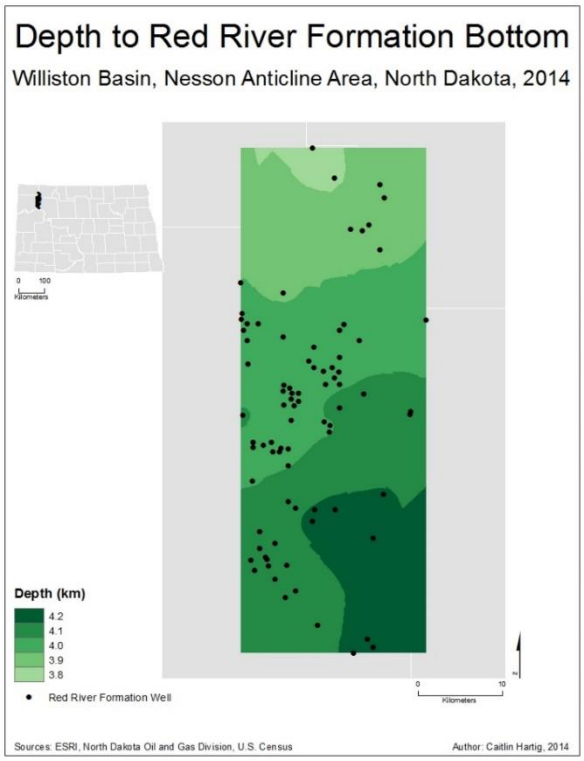

Figure 7: Depth to Red River Formation Bottom. Interpolation was completed using the Ordinary Kriging method; RMSE = 0.03770293.

To obtain the average unit thickness for the Red River Formation, the maximum thickness of the Red River Formation (213 m) was acquired from the North Dakota Geological Survey (NDGS) North Dakota Stratigraphic Column (Murphy et al., 2009). Next, TSTRAT (Temperature based on Stratigraphy) for NDGS Well 5086 (similar to that in Gosnold et al., 2012) was utilized to calculate a correction factor for the NDGS maximum thickness of the Red River Formation because the sum of the maximum thicknesses for the Williston Basin formations (6545 m) (Murphy et al., 2009) was greater than the TSTRAT depth to the bottom of the basin (4740 m) (Table 1, Appendix A). NDGS Well 5086 was used for this correction because 1) the well had similar formation depth and thickness to the study area, and 2) the well extended to the bottom of the basin.

It should be noted that all TSTRAT wells contain depth information from the North Dakota Oil and Gas Division website that has been extrapolated to reach the depth of the Precambrian Basement rocks based on the average unit thicknesses for each formation. For instance, NDGS Well 5086 only reaches the Red River Formation, but the depth of the stratigraphic column was projected to reach the Precambrian Basement by adding the maximum thicknesses of the Red River Formation and the Deadwood Formation (Murphy et al., 2009) to the depth to the top of the Red River Formation.

The correction factor was calculated in Equation 3:

$$Correction = \frac{z_b}{\sum z_{max}} \tag{3}$$

where z_b is depth to the bottom of the basin (NDGS Well 5086 TSTRAT) and $\sum z_{max}$ is the sum of the maximum thicknesses for the Williston Basin formations (Murphy et al., 2009).

$$Correction = \frac{4740\ m}{6545\ m}$$

$$Correction = 0.72$$

Subsequently, the maximum thickness of the Red River Formation (213 m) (Murphy et al., 2009) was multiplied by the correction factor of 0.72, which resulted in an average unit thickness of 0.154 km for the Red River Formation in the study area.

Consequently, 0.154 km was added to the depth to the top of the formation for each well in the study area to obtain an approximate depth to the bottom of the formation for the remaining 45 wells in the study area. The interpolation for depth to the bottom of the formation is shown in Figure 7. Along with the data for the depth to the top of the formation, the data for the depth to the bottom of the formation are listed in Table 2 in Appendix A.

Permeability was obtained from core analyses in the well log files on the North Dakota Oil and Gas Division website. Out of 81 total Red River Formation wells in the study area, only three wells-- 4379, 6915, and 1385—contained permeability data for the Red River Formation as a whole. In addition to permeability for the formation as a whole, wells 6915 and 4379 also contained permeability data specifically for Red River Formation Unit C. For the rest of the wells in the study area, only 8 had permeability data; those 8 measurements were all specifically for Red River Formation Unit C. Consequently, permeability of only Red River Unit C was interpolated (Figure 8); there were only 10 total measurements.

Because the permeability was interpolated specifically for Unit C, porosity was also interpolated specifically for Unit C for consistency. Porosity data of Unit C were ascertained from the Compensated Neutron Density (CND) logs when available (North Dakota Oil and Gas Division). When there was no CND log, the Borehole Compensated Sonic (BCS) log was utilized (North Dakota Oil and Gas Division) to obtain Δt_{log}, which was then input into Equation 4 to calculate the porosity:

$$\varphi_{sonic} = \frac{\Delta t_{log} - \Delta t_{ma}}{\Delta t_f - \Delta t_{ma}} \quad (4)$$

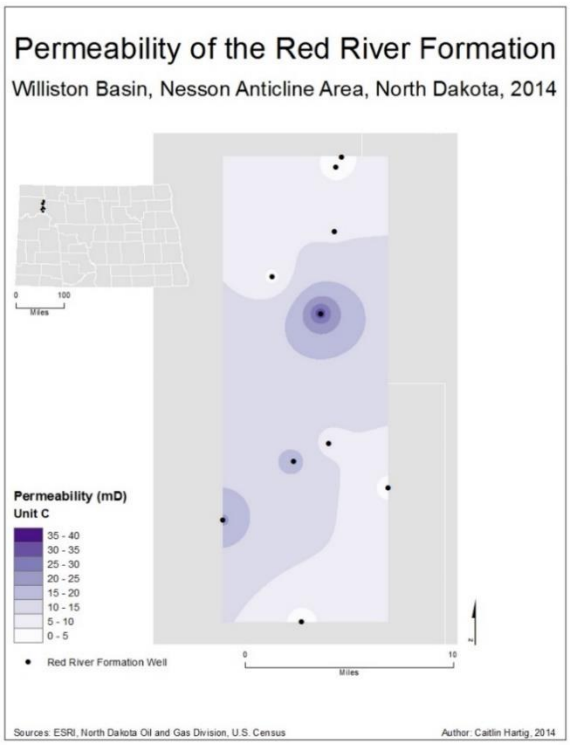

Figure 8: Permeability of the Red River Formation. Interpolation for Unit C was completed using the Inverse Distance Weighted (IDW) method; RMSE = 13.71893.

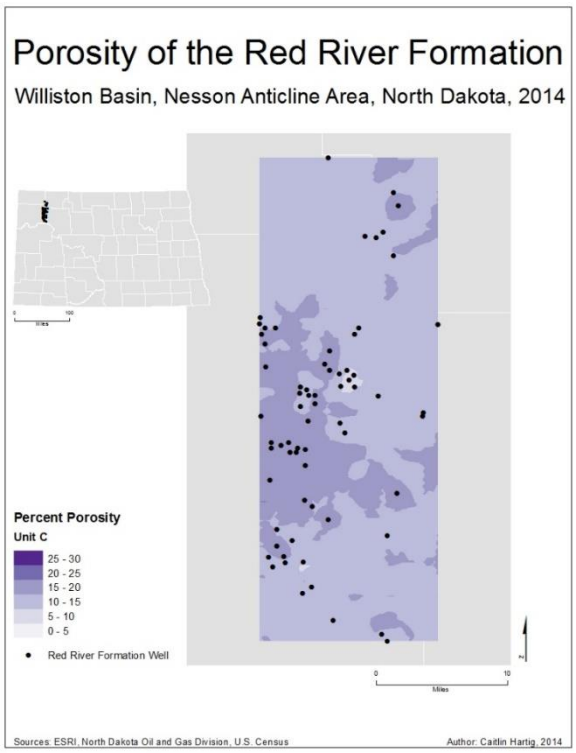

Figure 9: Porosity of the Red River Formation. Interpolation for Unit C was completed using the Ordinary Kriging method; RMSE = 0.05687078.

where φ_{sonic} is porosity, Δt_f is 185 (typical value for salt), Δt_{ma} is 43.5 (typical value for a limestone/dolostone lithology), and Δt_{log} is the result from the BCS log (Wyllie et al., 1958).

There were 66 porosity measurements in total. It was assumed that 1) the reservoir had a normal porosity distribution and 2) the porosity measurements included porosity of both the natural fractures and rock pores. The interpolation for porosity is shown in Figure 9. Along with the permeability data, the porosity data are listed in Table 2 in Appendix A.

Initially, heat flow was obtained from the National Geothermal Data System (NGDS) global heat flow spreadsheet. However, this dataset only provided 8 heat flow points that fell within the study area, which was not conducive to accurate interpolation. Furthermore, after the interpolation of surface heat flow was completed (Figure 10), a mistake in the data became apparent. Thus the NGDS dataset was not utilized for the remainder of the project.

Instead, the heat flow was calculated as follows. Bottom hole temperatures (BHT) for 50 of the 81 wells from the North Dakota Oil and Gas Division website were adjusted using the Harrison Correction (interpolation shown in Figure 11). Subsequently, the geothermal gradient was calculated for those 50 wells assuming a surface temperature of 6° C (interpolation shown in Figure 12). BHTs are listed in Table 4 in Appendix A.

Once the geothermal gradient was calculated, the heat flow of each well (50 wells total) was calculated using Fourier's Law (Equation 1). To use Fourier's Law, the thermal conductivity of the basin first needed to be ascertained. To calculate the thermal conductivity of the basin, Equations 5 and 6 were applied to the TSTRAT for NDGS Well 6840 (similar method to Gosnold et al., 2012), using the data from Table 3 in Appendix A. NDGS Well 6840 was used for this purpose because 1) the well had similar formation depth and thickness in comparison to the study area, and 2) the data was available for all formations in the basin.

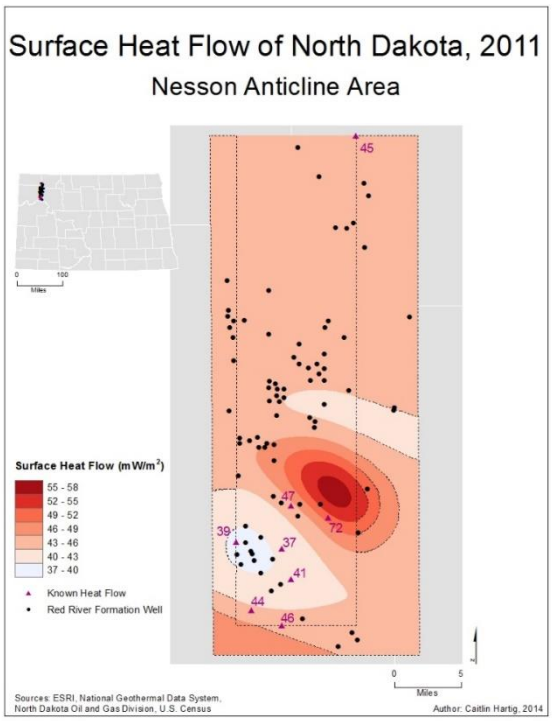

Figure 10: Surface Heat Flow of North Dakota. Data points were obtained for the Nesson Anticline Area from the NGDS global heat flow spreadsheet. Interpolation was completed using the Ordinary Kriging method; RMSE = 0.908885.

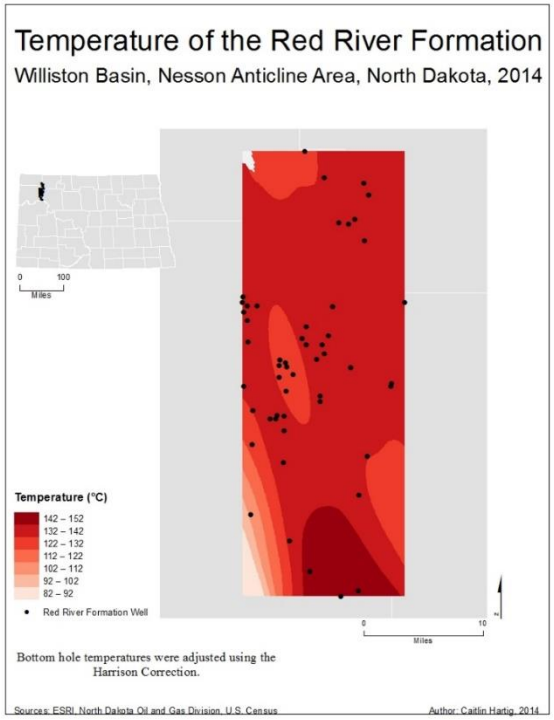

Figure 11: Temperature of the Red River Formation (BHT). Bottom hole temperatures were adjusted using the Harrison Correction. Interpolation was completed using the Ordinary Kriging method; RMSE = 10.13062.

First, the Harmonic Mean Conductivity (HMC) of each formation was obtained using Equation 5:

$$HMC = \frac{z}{\lambda} \quad (5)$$

where *HMC* is Harmonic Mean Conductivity of each formation (K/m), *z* is formation thickness (m), and λ is formation thermal conductivity (W/mK). Thermal conductivities of each formation were measured from core samples provided by the North Dakota Geological Survey (NDGS) with a divided bar apparatus, and the stratigraphic section was constructed from the North Dakota Oil and Gas Division website (William Gosnold, Pers. Comm., 2015).

Subsequently, Equation 6 was utilized to calculate the thermal conductivity of the Williston Basin as a whole (λ_{basin}):

$$\lambda_{basin} = \frac{\sum z}{\sum HMC} \quad (6)$$

$$\lambda_{basin} = 1.667 \text{ W/mK}$$

where λ_{basin} is thermal conductivity of the basin (W/mK), $\sum z$ is the sum of all formation thicknesses (m), and $\sum HMC$ is the sum of all formation HMC. Once the thermal conductivity of the basin had been computed, heat flow was then calculated using Equation 1. The geothermal gradients used for this calculation are listed in Table 4 in Appendix A.

Subsequently, the heat flow results were interpolated in Figure 13 (circles). 32 Red River Formation wells did not have bottom hole temperatures available; because of this, heat flow could not be calculated for those wells. To ameliorate this problem, heat flow for these 32 wells was predicted from the well placement on Figure 13 (triangles). The heat flow measurements for all wells are listed in Table 4 in Appendix A.

Once the heat flow had been ascertained for all 81 wells in the study area, the results were input into an Excel model of NDGS Well 2894 TSTRAT (method similar to Gosnold et

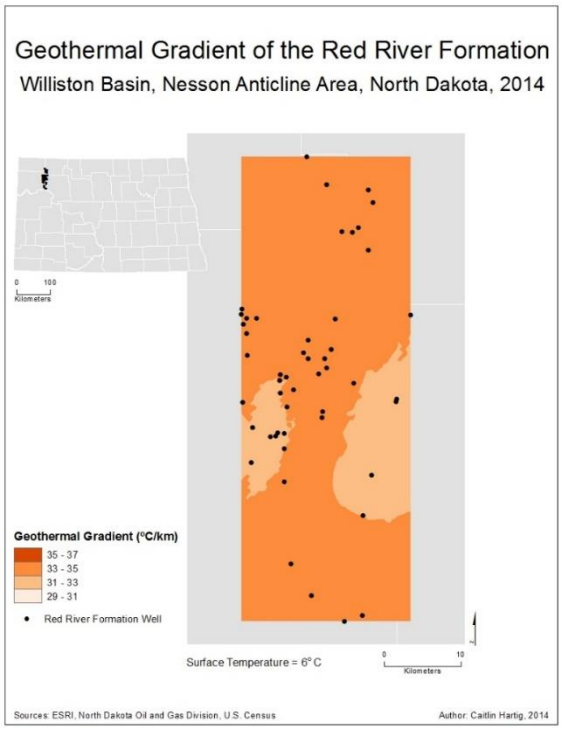

Figure 12: Geothermal Gradient of the Red River Formation. A surface temperature of 6° C was used. Interpolation was completed using the Ordinary Kriging method; RMSE = 1.622047.

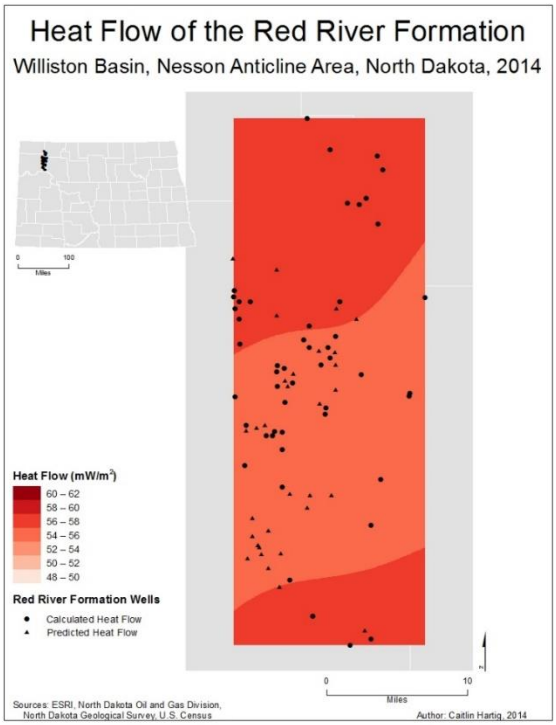

Figure 13: Heat Flow of the Red River Formation. Interpolation was completed using the Ordinary Kriging method; RMSE = 2.719738.

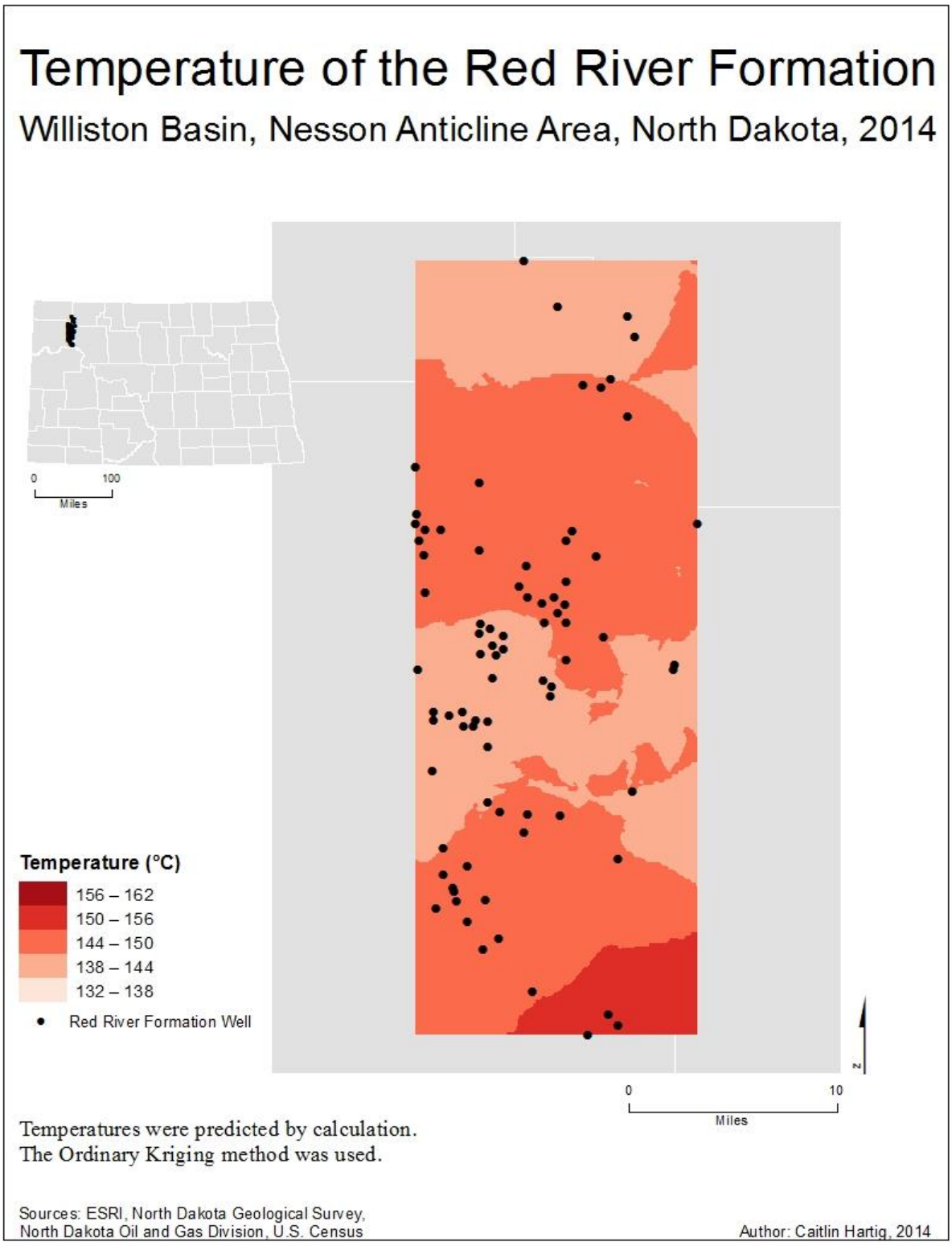

Figure 14: Temperature of the Red River Formation (Ordinary Kriging). Temperatures were calculated using thermal properties of rocks in the basin and heat flow. Interpolation was completed with the Ordinary Kriging method; RMSE = 4.987412.

al., 2012) to calculate the temperature of the Red River Formation for all wells using Equation 2. NDGS Well 2894 was used for this purpose because 1) the well had similar formation depth and thickness in comparison to the study area, and 2) the data was available for all formations in the basin. Before the depths to the Red River Formation in the study area were input into the Excel model, they were divided by 3989 m-- the depth to the top of the Red River Formation listed in NDGS Well 2894 TSTRAT-- to correct for the difference in depth between the model and the wells in the study area. The resulting temperatures are listed in Table 4 in Appendix A and the interpolation is shown in Figure 14.

Once temperature had been calculated for all Red River Formation wells, a Moran's I analysis was completed in order to confirm that the temperature data were clustered (Figure 15). A Moran's I analysis is a geostatistical method used in ArcGIS to calculate the spatial autocorrelation of a dataset in order to determine whether that dataset is random, dispersed, or clustered. It was predicted that the temperature data would show clustering because the depth to the top of the formation and the heat flow are both input parameters that influence the temperature in the subsurface, as shown by Equation 2. The fact that the temperature data showed clustering in the

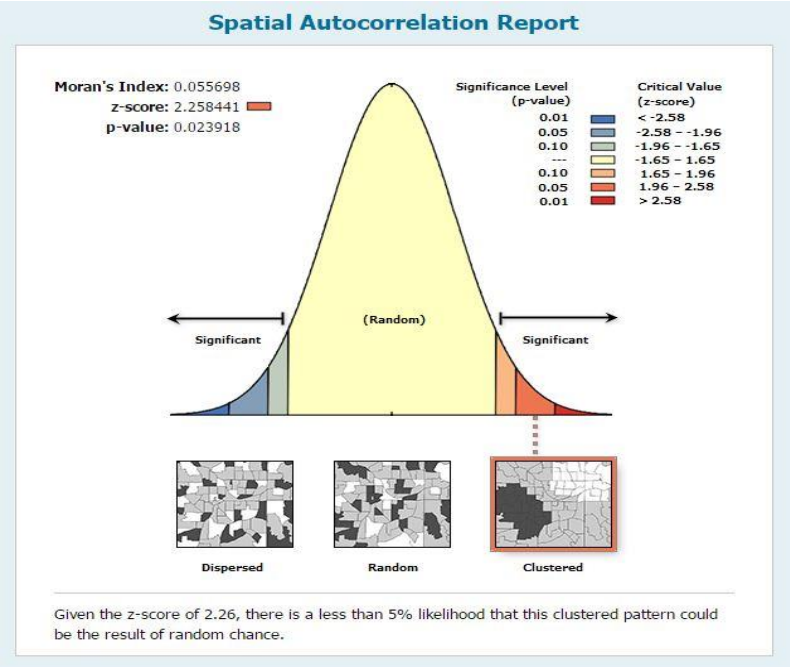

Figure 15: Moran's I Analysis of the Calculated Temperatures shows that the data are clustered and are thus not likely to be the result of random chance.

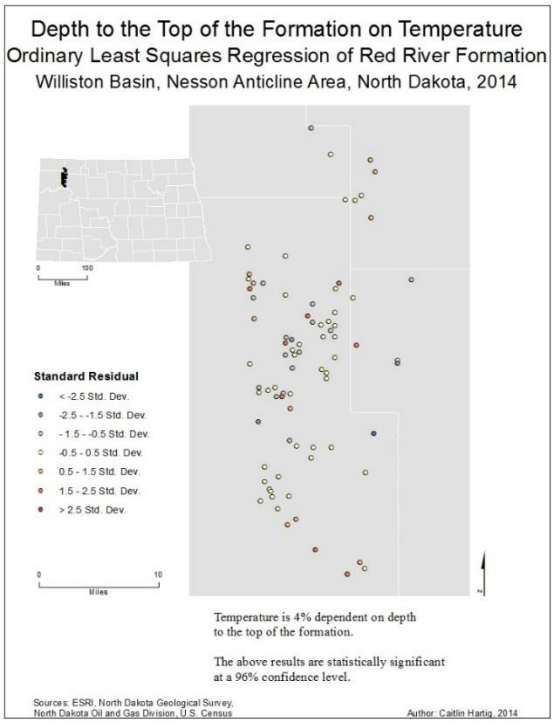

Figure 16: Depth to the Top of the Formation on Temperature (OLS). Temperature is 4% dependent on depth to the top of the formation.

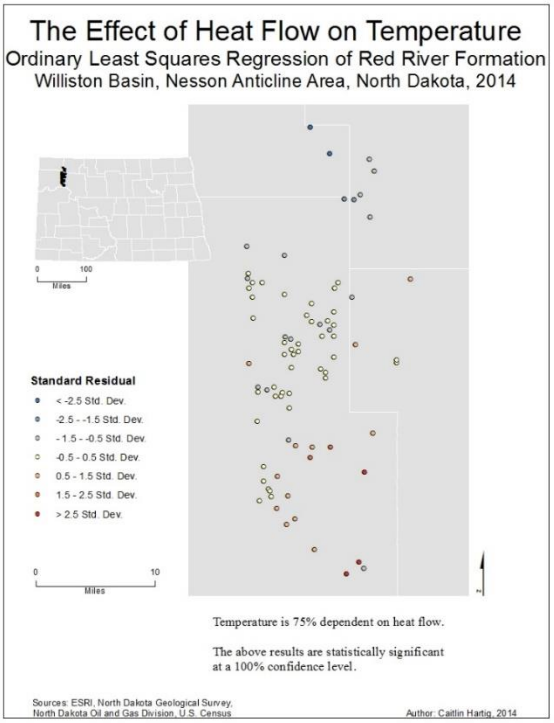

Figure 17: The Effect of Heat Flow on Temperature (OLS). Temperature is 75% dependent on heat flow.

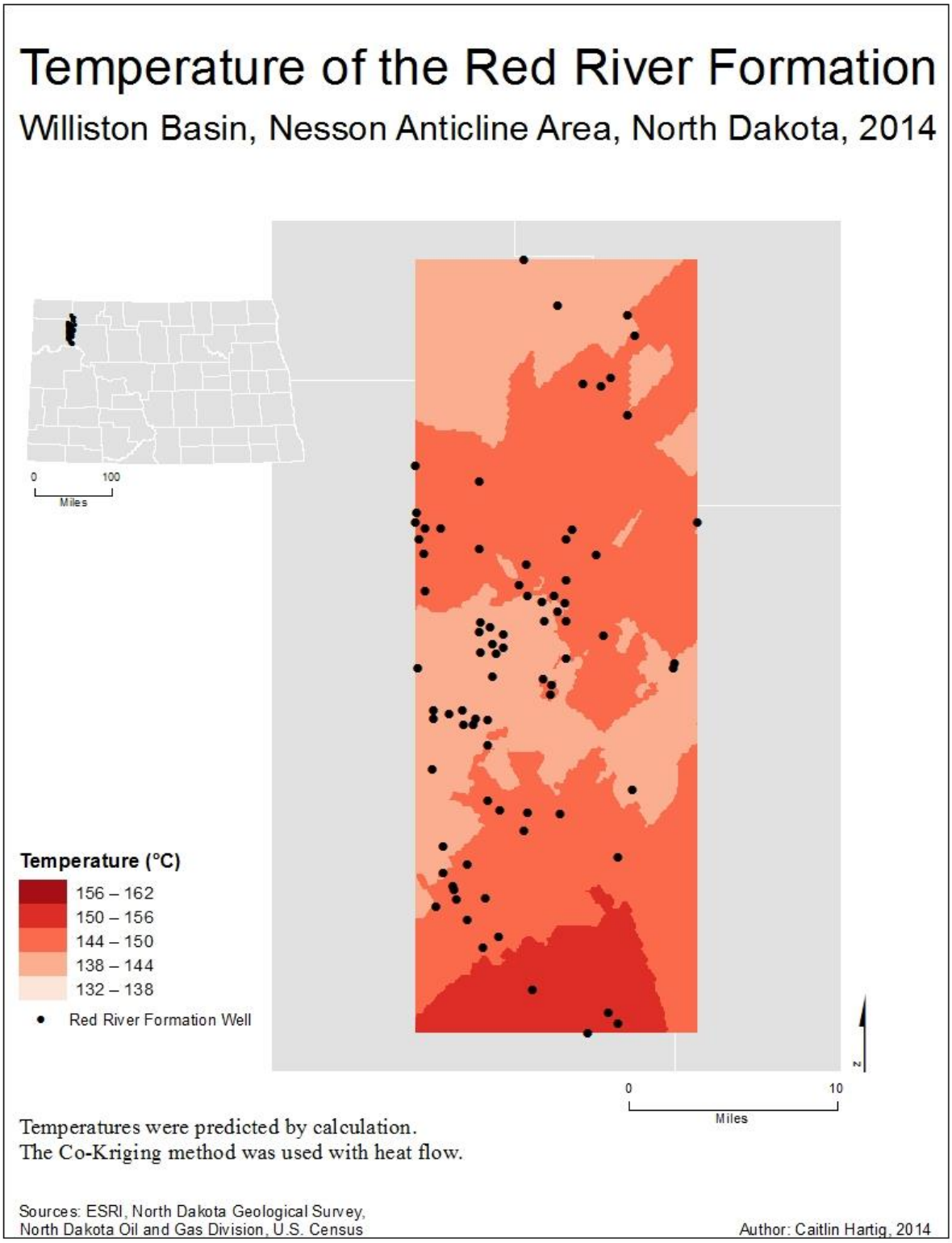

Figure 18: Temperature of the Red River Formation (Co-Kriging). Temperatures were calculated using thermal properties of rocks in the basin and heat flow. Interpolation was completed with the Co-Kriging method utilizing heat flow; RMSE = 1.925584.

Moran's I confirmed that the model was working correctly and that there were sufficient data points to complete the analysis.

Subsequently, Ordinary Least Squares (OLS) regressions showed that the influence of heat flow on the formation temperatures was more than 18 times stronger than the influence of depth to the top of the formation on the formation temperatures. Figure 16 shows that depth to the top of the formation only influences the formation temperature by 4%, while Figure 17 shows that heat flow influences the formation temperatures by 75%. Consequently, heat flow is a far more significant control on the formation temperatures than depth.

Based on these results, a Co-Kriging interpolation of temperature was completed with heat flow and is shown in Figure 18. A Co-Kriging interpolation differs from an Ordinary Kriging interpolation in that the Co-Kriging method calculates the semivariance of two variables (one independent and one dependent), while the Ordinary Kriging interpolation only calculates the semivariance of one variable. In this case, temperature was the dependent variable and heat flow was the independent variable. The model calculated the formation temperatures by considering the effects of heat flow at each well location.

Discussion

Upon examining the surface heat flow interpolation in Figure 10, it is apparent that there is a faulty data point in the NGDS spreadsheet. A surface heat flow value of 72 mW/m^2 cannot logically be found so close to a surface heat flow value of 47 mW/m^2. Because the surrounding heat flow values are much lower, the faulty point must be that with 72 mW/m^2.

Additionally, the presence of bull's-eyes in Figure 10 indicates that 8 data points are too few to produce an accurate interpolation. The bull's-eye problem is also apparent in the

permeability interpolation (Figure 8) (10 data points) and the corrected BHT interpolation (Figure 11) (50 data points). Consequently, these three interpolations should not be utilized.

Furthermore, there is a hint of distortion (jagged edges) on the southeast and northeast corners of the Co-Kriging interpolation of the temperature with heat flow (Figure 18). In spite of this, there is not so much distortion present that the interpolation should be discarded.

Because the Co-Kriging result (Figure 18) has the lowest RMSE out of the three temperature interpolations, it is a viable temperature prediction. The Ordinary Kriging of calculated temperatures (Figure 14) has no distortion and is therefore also a viable temperature prediction, despite having a higher RMSE by a factor of more than 2.5.

Because the interpolation of the bottom hole temperatures (Figure 11) has an RMSE twice as high as the Ordinary Kriging interpolation, it is evident that calculation of subsurface temperatures based on heat flow and thermal properties is a more effective method than just simply correcting and interpolating BHTs.

Conclusion

GIS analysis has been completed to produce interpolations of depth to the top of the formation, depth to the bottom of the formation, permeability, porosity, geothermal gradient, heat flow, and temperature. The interpolations for depth to the top of the formation (Figure 6), depth to the bottom of the formation (Figure 7), porosity (Figure 9), geothermal gradient (Figure 12), and heat flow (Figure 13) are all acceptable results for input into a reservoir simulation model. All that can be said for permeability is that it varies from 0.1-38 mD in the limestones; the interpolation was inadequate due to a scarcity of data. Both the interpolation of the calculated temperatures (Figure 14) and the interpolation of calculated temperatures

with the influence of heat flow (Figure 18) are acceptable predictions for the subsurface temperatures that can be utilized in a reservoir simulation model.

Upon examining both Figures 14 and 18, it is apparent that the hottest section of the region is in the south-central part of the study area. According to Figure 14, temperatures of 150-156° C are found in the southeastern corner of the study area (extending from the eastern edge of Williams County into western Mountrail County). This hot section extends 9.8 km horizontally and 8.0 km vertically. According to Figure 18, temperatures of 150-156° C are found in the southwestern and south-central part of the study area (contained within Williams County). This hot section extends 13.6 km horizontally and 9.9 km vertically. Regardless of which temperature map is utilized, the southeastern section of Williams County has the hottest temperatures, and is therefore the best place to install an SEGS in the study area.

It should be noted that there may be some interference from glacial isostasy in the region; therefore, all temperatures shown in Figures 14 and 18 may be up to 15° too warm. Consequently, it can only be said with certainty that the hottest temperatures surpass 140° C.

CHAPTER III

RED RIVER FORMATION NATURAL FRACTURE ANALYSIS

Natural Fracture Data

To understand the natural fracture orientation and location in the Red River Formation, existing data was first examined. Unfortunately, seismic data were unavailable for this study and therefore could not be utilized. Additionally, core images only existed for a mere four wells in the study area (North Dakota Oil and Gas Division). While the cores showed where the natural fractures intersected the wells, they were unoriented; as a result of this, it was impossible to ascertain the natural fracture orientation from the core images.

As a result of this paucity of data, it was necessary to utilize literary analyses of the Williston Basin's stress field orientation, known natural fracture orientations, and surface lineament orientations to deduce the natural fracture orientation of the study area.

Stress Regime and Natural Fracture Orientation

Natural fracture orientation can be inferred from the regional stress field. The stable interior of North America—including the central and eastern United States, most of Canada, and most of the western Atlantic—has been classified into the Midplate stress province (M.D. Zoback and M.L. Zoback, 1991). The Midplate stress province is characterized by a compressive stress regime of strike-slip and reverse faulting in which $S_{Hmax} > S_V > S_{Hmin}$ in the United States (primarily-strike slip faulting) and $S_{Hmax} > S_{Hmin} > S_V$ in Canada (primarily reverse faulting) (M.D. Zoback and M.L. Zoback, 1991; M.L. Zoback and M.D. Zoback, 1989). The cause of this stress regime has been attributed the absolute plate motion of the

North American plate to the Southwest, as well as to the ridge-push motions from the Mid-Atlantic ridge (Bell and Grasby, 2012; M.L. Zoback and M.D. Zoback, 1989).

M.D. Zoback and M.L. Zoback, 1991 and Bell and Grasby, 2012 came to the above conclusions from analyzing well bore breakouts. Well bore breakouts are anisotropic cavities that occur on opposite sides of a borehole wall when the well is distorted as a result of stress (Bell and Grasby, 2012). The breakouts are oriented in the direction of S_{Hmin}, where the elastic compressive stress concentration is the greatest (Zoback et al., 1985).

M.D. Zoback and M.L. Zoback, 1991 analyzed the well bore breakouts with an ultrasonic borehole televiewer. A televiewer is a well-logging tool that contains a magnetically orientated rotating piezoelectric transducer that emits and receives an ultrasonic (~1 MHz) acoustic pulse that is reflected from the borehole wall at 600 times per revolution (Zoback et al., 1985). The televiewer shows the fractures that intersect the well bores as a function of azimuth and depth, based on the reflectivity of the well bore; the reflected pulse is shown as brightness on a three-axis oscilloscope and yields an "unwrapped" image of the well bore surface (Zoback et al., 1985). One well was analyzed near Auburn, New York and showed a 6.5-m long zone of breakouts in the well bore centered at a depth of 1476.3 m in a Paleozoic sandstone (Zoback et al., 1985). Another well was analyzed near Monticello, South Carolina and showed a 7.5-m long zone of breakouts in the well bore centered at a depth of 794.5 m in a granite (Zoback et al., 1985). Other break outs were similarly analyzed in the southeastern corner of Saskatchewan (M.L. Zoback and M.D. Zoback, 1989), which is ~100 kilometers away from the current study area in western North Dakota.

Bell and Grasby, 2012 analyzed the well bore breakouts with a 4-arm dipmeter imagery log for Mesozoic and Paleozoic shales, limestones, and dolostones. A dipmeter is an

instrument that documents the cavities on opposite sides of the well bore in order to ensure that the lateral elongation of the borehole was caused by stress caving (Bell and Grasby, 2012). A dipmeter works by recording the extensions of opposing pairs of pads, in addition to the compass orientation of one of the pads (Bell and Grasby, 2012). One well analyzed was in northern Alberta and showed twenty-three ~254.8-m thick breakout intervals in the well bore that were centered at a depth of 3496.35 m (Bell and Grasby, 2012). Only ten measurements total were available in western Canada (Bell and Grasby, 2012).

The results of both of the above well bore breakout analyses showed a maximum horizontal stress (compression) (S_{Hmax}) oriented in the east/northeast direction and a minimum horizontal stress (compression) (S_{Hmin}) oriented in the north/northwest direction (M.D. Zoback and M.L. Zoback, 1991; Bell and Grasby, 2012). Because S_{Hmax} is oriented northeast/southwest, the natural fracture orientation can be inferred to also be oriented northeast/southwest.

In other studies, there is an opposing viewpoint that local stresses, rather than tectonic movements, are responsible for the stress regime in the Williston Basin. These studies propose that the Nesson Anticline was formed along reactivated basement block boundaries in response to varying tectonic stresses and crustal flexure that occurred intermittently throughout the Phanerozoic (LeFever et al., 1987; Freisatz, 1995; Laird and Folsom, 1956). In essence, these studies suggest that the stress regime of the Williston Basin is extensional, rather than compressional.

LeFever et al., 1987 examined structural relief plots and split the area of the Nesson Anticline into nine distinct areas, each of which having its own independent structural history. Episodes of alternating uplift and subsidence occurred in each of these blocks in

different intervals over the Phanerozoic (LeFever et al., 1987). Most of these areas experienced the largest amount of uplift in the Devonian or in the Early Mississippian, while a few of these areas did not experience the largest amount of uplift until the Pennsylvanian (LeFever et al., 1987). These results agree with the ideas of Laird and Folsom, 1956, who believe that the Nesson Anticline formed sometime in the late Ordovician and became more active at the end of the Paleozoic.

Other studies have been completed in the Canadian Williston Basin in Saskatchewan and Manitoba to determine the natural fracture orientation in the subsurface of the Williston Basin. In the Torquay-Rocanville trend near the Weyburn oil field in southeast Saskatchewan, the flow of oil has been determined to be in a preferential northeast-southwest orientation (Chen et al., 2009). As a result, it is suggested that natural fractures in the area have a dominant northeast-southwest orientation (Chen et al., 2009). Furthermore, a carbonate aquifer in southern Manitoba (middle Ordovician to Devonian) shows two dominant fracture orientations observed in bedrock exposures: northeast-southwest (020°-040°), and northwest-southeast (110°-130°) (Chen et al., 2011) or the equivalent (290°-310°). The northwest trending group (perpendicular to S_{Hmax} and parallel to S_{Hmin}) has a higher fracture density, but consists of mostly healed or closed fractures (Chen et al., 2011). The northeast trending group (parallel to S_{Hmax}) has a significantly higher permeability and is the preferential fluid-flow pathway (Chen et al., 2011; Wegelin, 1987).

Fluid in the subsurface should theoretically flow preferentially in the direction of maximum stress, regardless of whether that stress is horizontal or vertical. Because Chen et al., 2011 and Wegelin, 1987 observed the subsurface fluid to flow in a preferential northeast direction, it can be assumed that the direction of maximum stress in the subsurface is oriented

to the Northeast (a horizontal stress). As a result of this information, it can be deduced that the direction of maximum horizontal stress (S_{Hmax}) is oriented to the Northeast and that S_{Hmax} is greater than the vertical overburden stress (S_V). These findings suggests that the stress of the region is $S_{Hmax} > S_{Hmin} > S_V$, a compressive regime, which is consistent with the results of Bell and Grasby, 2012 and M.D. Zoback and M.L. Zoback, 1991. If the stress regime were extensional, on the other hand, then $S_V > S_{Hmax} > S_{Hmin}$ (Zoback, 1989). Thus the stress field of the United States craton is a compressive regime that is caused by the northeastern movements of the North American plate and the spreading of the Mid-Atlantic ridge.

To sum up, the consistent findings of Chen et al. 2011, Wegelin, 1987, Bell and Grasby, 2012, and M.D. Zoback and M.L. Zoback, 1991 show that the natural fractures in the subsurface of the Williston Basin are oriented northeast and northwest and that the northeast trending group is the conduit for fluid flow. This information is applicable to the natural fracture orientation in the Nesson Anticline area of the basin in North Dakota.

Surface Lineament Orientation

In addition to the two directions of natural fractures obtained from the Canadian studies, there are also two distinct surface lineament (joint) zones in the area that are coincidentally also trending northeast and northwest. Northeast and northwest trending lineaments have been observed across Winnipeg (Chen et al., 2011) as well as in the Nesson Anticline area and Mountrail County, North Dakota (Anderson, 2011; Gerhard et al., 1987).

It has been argued that surface lineament orientation can reflect the orientation of the basement faults in the subsurface, and therefore by extension can reflect the specific orientations and locations of the natural fractures in the formation (Bell and Grasby, 2012; Anderson, 2011; Penner, 2006; Freisatz, 1995; Freisatz, 1991; Gerhard et al., 1987). The

assumptions are 1) that the basement faults cut through the subsurface formation in question, 2) that the trends of the natural fractures in the subsurface are parallel to the trends of the basement faults, and 3) that the surface lineaments are formed either a) by the motion of the basement faults, or b) by the same source that formed the basement faults. It has also been proposed that the surface lineaments are vertically connected to the basement faults as fault traces (Anderson, 2011; Chen et al., 2011; Freisatz, 1995).

In spite of the similarities in trend between the basement faults and the surface lineaments, advances and retreats of Pleistocene glacial till show "ridge and swale" topography that is also nearly coincident with the inferred direction of preferred fracture orientations (Chen et al., 2011; Gerhard et al., 1990). Furthermore, Cenozoic detrital sedimentary rocks can mask the geologic expression of the basin (Gerhard et al., 1990). Because of this, lineaments may not be able to adequately predict the orientations of the subsurface features (Chen et al., 2011; Gerhard et al., 1990; Gerhard et al., 1987).

Research Question

A paucity of natural fracture orientation data in the subsurface impedes immediate understanding of the natural fracture orientation of the study area in western North Dakota. While there are many known surface lineaments in the area and some known basement faults, it is disputed that the surface lineaments are, in actuality, caused by the basement faults. Thus it is uncertain whether or not it can be said with confidence that the surface lineaments reflect the orientations and locations of the natural fractures in the subsurface.

As a result of this uncertainty, it was necessary to conduct a GIS and geostatistical analysis comparing the trends of the surface lineaments to the trends of the basement faults in order to determine whether or not they are sufficiently correlated. In the event that a strong

spatial autocorrelation were found to exist between the trends of the surface lineaments and the trends of the basement faults, the approximation of the specific natural fracture orientations and locations in the Red River Formation would be greatly facilitated.

GIS and Geostatistical Analysis

To begin the GIS and geostatistical analysis, two distinct shapefiles were needed: one containing the spatial distribution of the surface lineaments and the other containing the spatial distribution of the subsurface basement faults. The first shapefile was spatially referenced and digitized by Fred Anderson and Elroy Kadrmas, 2011; it contained the spatial distributions of all historic surface lineaments in the Williston 250k from Cooley, 1983 and other sources. Lineaments in this file were derived from four distinct sources: 1) previous studies, 2) digital shaded relief data, 3) aerial imagery, and 4) LANDSAT data/imagery (Anderson, 2008). The second shapefile was a diagram of basement faults in Mountrail County, North Dakota (Anderson, 2011) that was georeferenced to a shapefile of Mountrail County (United States Census, 2014) and digitized into a separate layer. The basement faults have been identified from seismic data (Anderson, 2011).

Once the two distinct shapefiles were obtained and created, respectively, the linear directional mean tool and the directional distribution tool were run on both layers in ArcGIS (Figure 19). The surface lineaments trend in two distinct directions (northwest and northeast); therefore, the results of the linear directional mean and the directional distribution were not included on the map because they did not reflect both directional trends.

Subsequently, Moran's I analyses (Figures 20-21) were run on the lineaments and the faults. From the clustered results, it is unlikely that either the lineaments or the faults were formed by random chance.

Next, the trends for each distinct surface lineament and each distinct basement fault were obtained for the geostatistical analysis with the linear directional mean tool. Compass plots were created in MATLAB to analyze the relationships between the basement fault trends and the surface lineament trends (Figures 22-25). Finally, the results were compared to determine whether the spatial autocorrelation was strong enough to argue common causality.

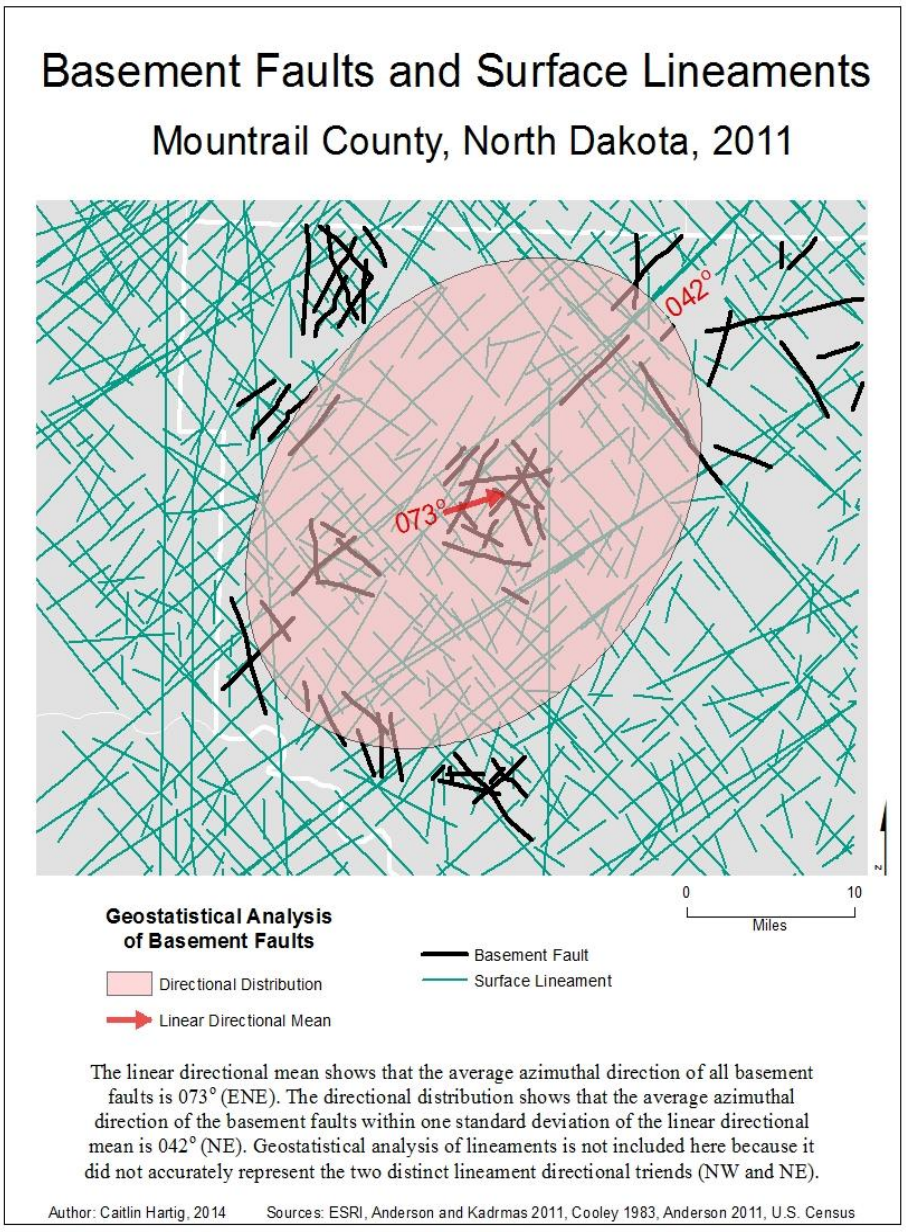

Figure 19: Basement Faults and Surface Lineaments. Shows features for Mountrail County, North Dakota, 2011.

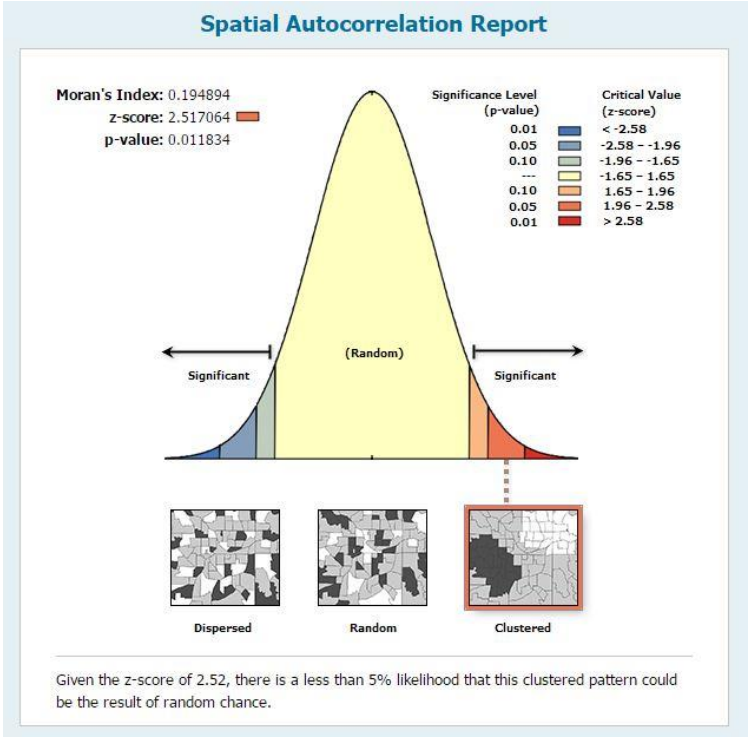

Figure 20: Moran's I Analysis of the Basement Faults shows that the data are clustered; therefore it is unlikely that they are the result of random chance.

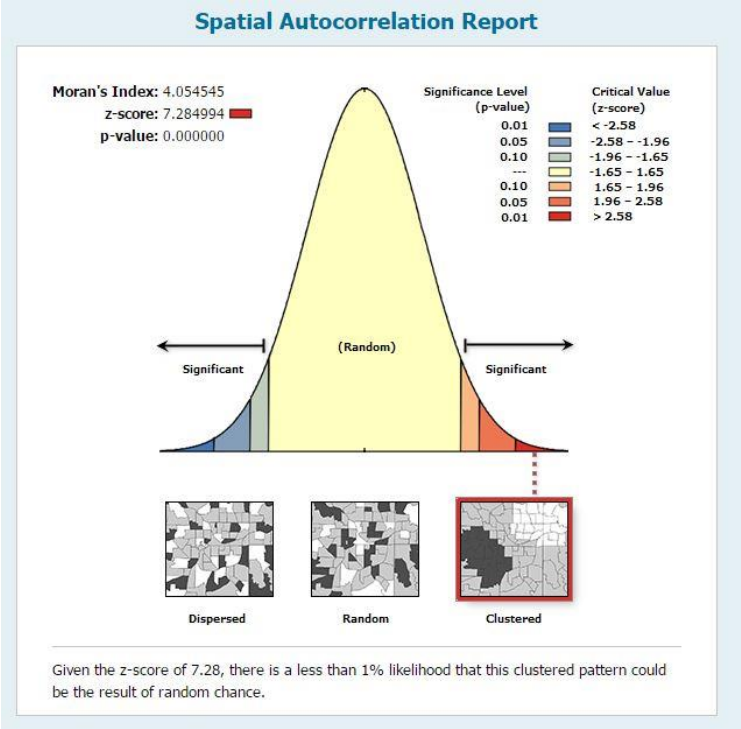

Figure 21: Moran's I Analysis of the Surface Lineaments shows that the data are clustered; therefore it is unlikely that they are the result of random chance.

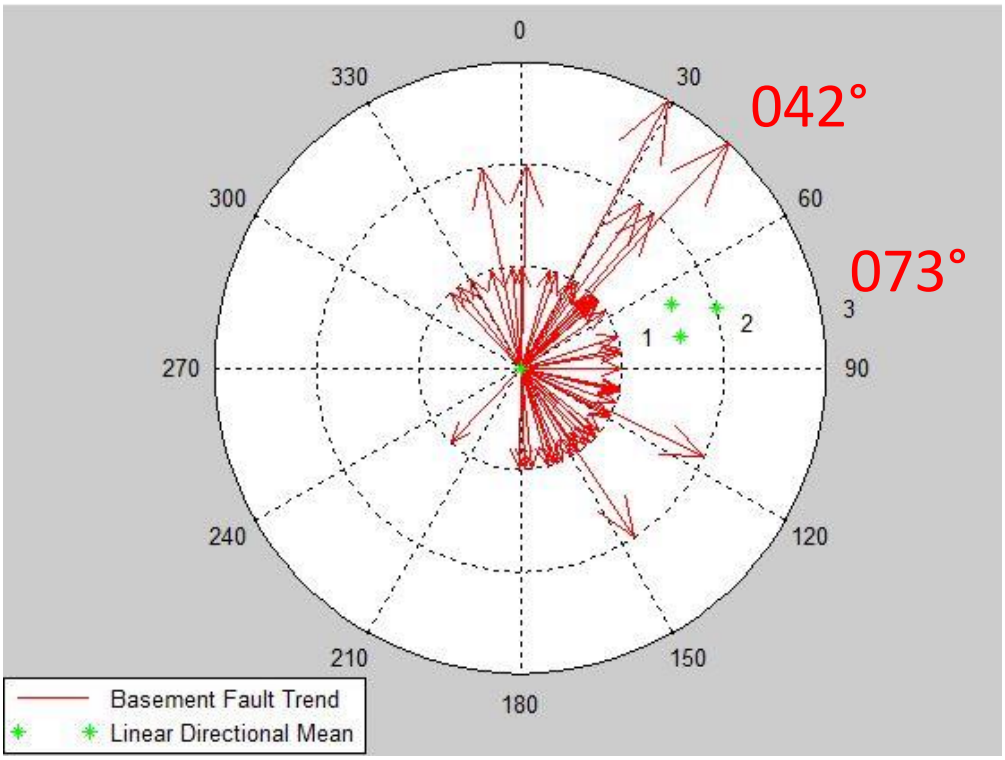

Figure 22: Compass Plot of the Basement Fault Trends shows an average ENE trend. The fault density is greatest at 042°, which is coincident with the directional distribution calculated in Figure 19. The linear directional mean calculated in Figure 19 (green stars) is pictured at 073°.

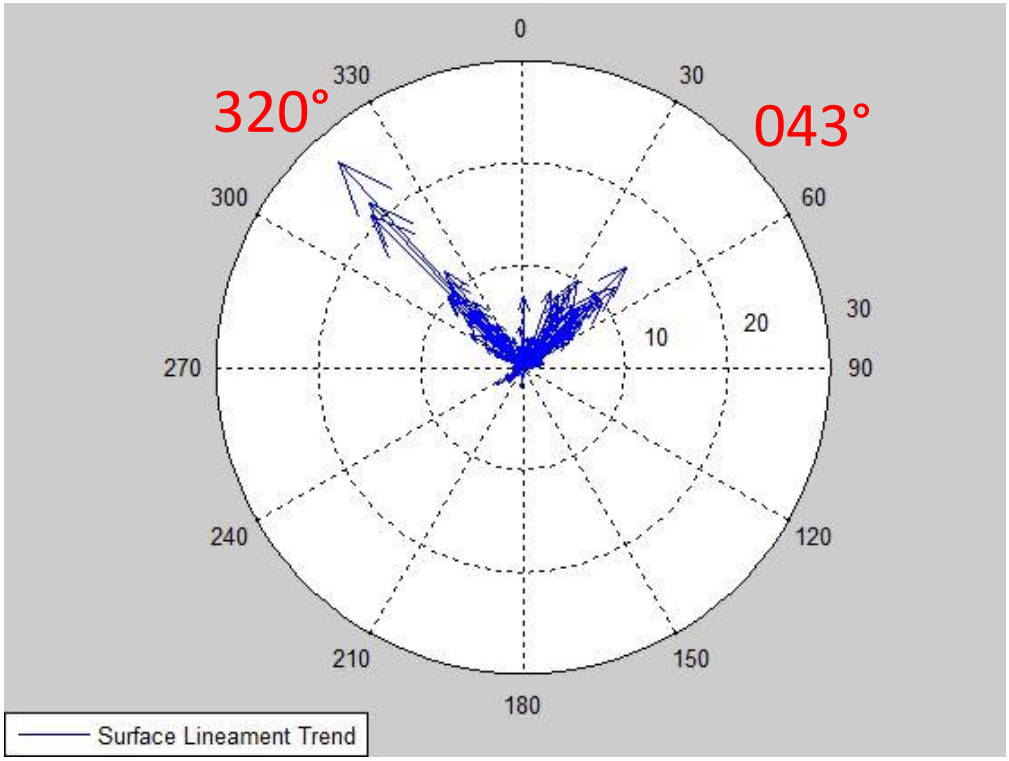

Figure 23: Compass Plot of the Surface Lineament Trends shows two distinctive trends: 320° (NW) and 043° (NE). Lineament density is greater in the northwest direction.

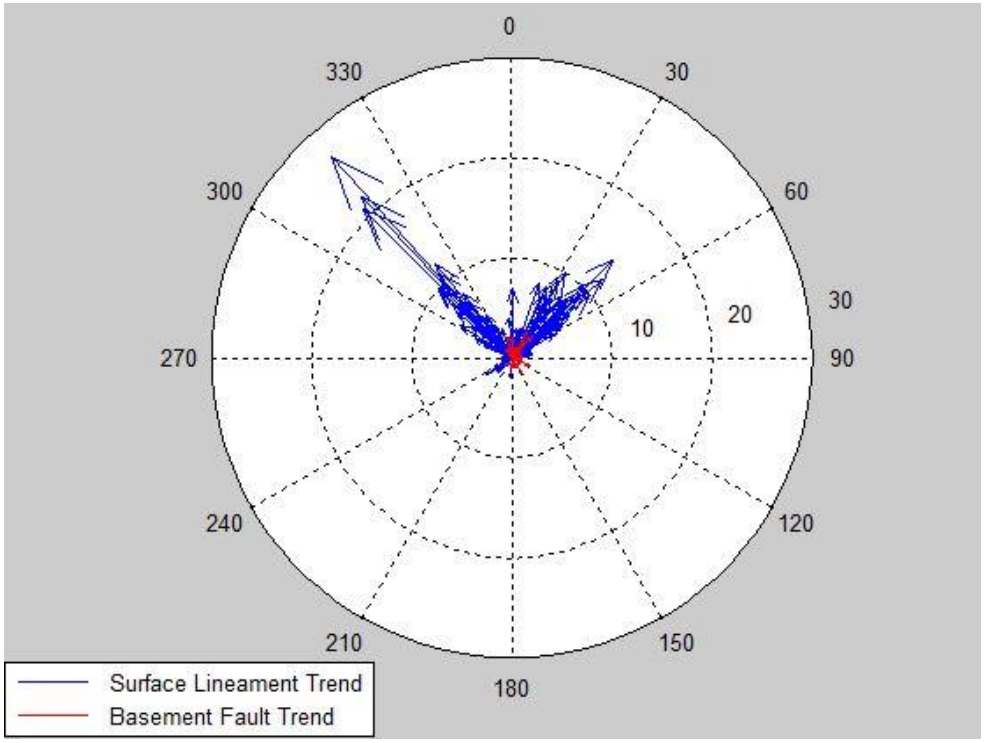

Figure 24: Compass Plot of the Basement Fault Trends and the Surface Lineament Trends. The large magnitude of lineaments and the small magnitude of faults makes comparison difficult.

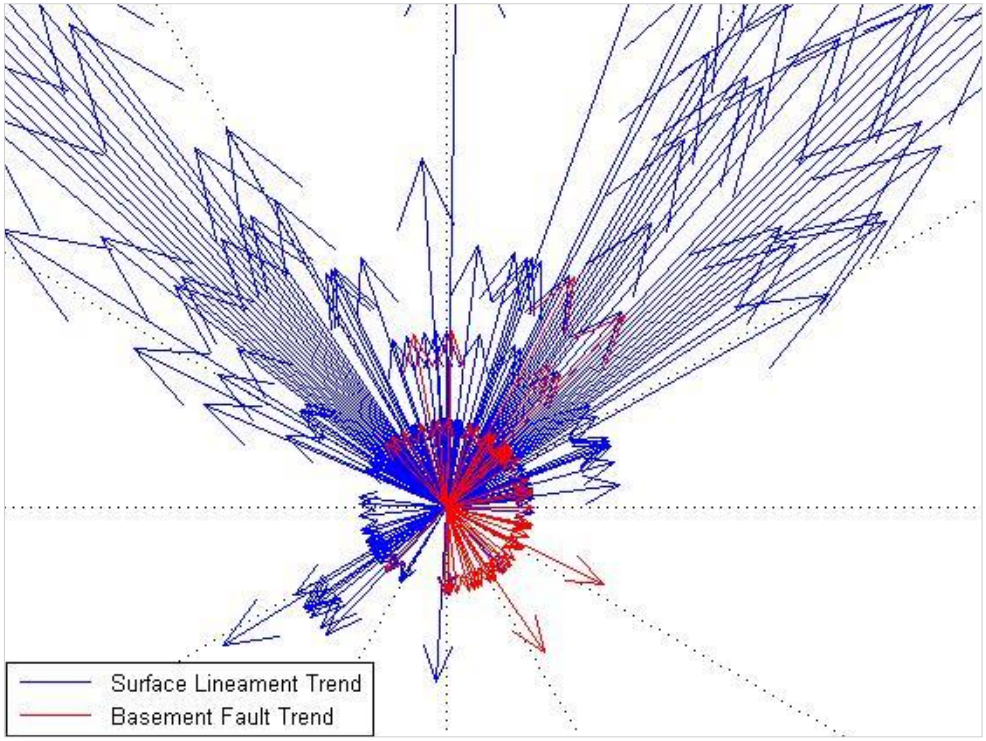

Figure 25: Figure 24, Zoomed In. The closer view facilitates comparison.

Discussion

The average azimuthal direction of all subsurface faults, 073° (Figures 19 and 22), is exactly coincident with the direction parallel to the regional stress field, S_{Hmax}, which is oriented ENE in this area. The clustering shown in the Moran's I analysis for the faults (Figure 20) is thus explained because the regional stress field likely caused the faults to form.

The compass plot of the surface lineaments in Figure 23 shows two distinct directions of trend: 320° (NW) and 043° (NE). The lineaments thus formed in the directions parallel both to S_{Hmin} and S_{Hmax} of the regional stress field, respectively. Furthermore, the azimuthal direction of lineaments trending northeast (043°) (Figure 23) is almost exactly coincident with the azimuthal direction of most subsurface faults (042°) (Figure 22). Therefore, the clustering shown in the Moran's I analysis for the lineaments (Figure 21) is thus explained because the regional stress field likely caused the faults to form, and then the faults likely caused the lineaments to form.

Conclusion

A dearth of available seismic data in western North Dakota and a lack of oriented cores hindered the immediate understanding of the natural fracture network present in the Red River Formation. As a result of this, studies in the Williston Basin of the regional stress field, natural fracture orientation, and surface lineament trends provided guidance in deducing the orientation and location of the natural fractures in the subsurface of the Red River Formation. The GIS and geostatistical analysis of the surface lineaments and the basement faults in Mountrail County, North Dakota, showed that there is sufficient spatial autocorrelation between the surface lineaments and the basement faults. It can thus be argued that the regional stress field caused the faults to form, and that the fault movements subsequently caused both the natural fractures and the surface lineaments to form. Because

the stress field is consistent over the study area, it can be assumed that the same relationships apply to the lineaments and faults in the adjacent Burke, Divide, and Williams counties.

As a result of this correlative relationship between the surface lineaments, basement faults, and natural fractures, it can be assumed that the surface lineaments mimic the underlying orientations and locations of both the basement faults and the natural fractures in the subsurface. According to Anderson, 2011, there are four different types of relationships between surface lineaments and basement faults: coincident, adjacent, bridging, and extending; furthermore, the basement faults are assumed to be subvertical (+/- 6 degrees from vertical) (William Gosnold, Richard LeFever, Fred Anderson, and Stephan Nordeng, Pers. Comm., 2014). The geometry of these relationships is summarized in Figure 26.

In all four relationships shown in Figure 26, the lineament trends are coincident with the fault trends. Therefore, due to lack of more exact information regarding the specific natural fracture orientation and location in the subsurface, it can be assumed that the surface lineaments and natural fractures are coincident in terms of orientation and location. Consequently, the natural fractures in the study area will be assumed to trend in the same directions as the surface lineaments: 320° (NW) and 043° (NE), on average.

In agreement with the ideas of Chen et al., 2011 and Wegelin, 1987, the natural fracture density is significantly greater in the northwest direction (S_{Hmin}) than in the northeast direction (Figure 23). On the other hand, the natural fractures trending to the Northeast (S_{Hmax}) are fewer in number but will be the conduits for flow. Because of this, it was suggested that the northeast trending fractures are more likely to remain open with the addition of fracture stimulation (Chen et al., 2011). Therefore, the hydroshearing dilation axis would be parallel to S_{Hmax} in the northeast direction (Bell and Grasby, 2012). Furthermore,

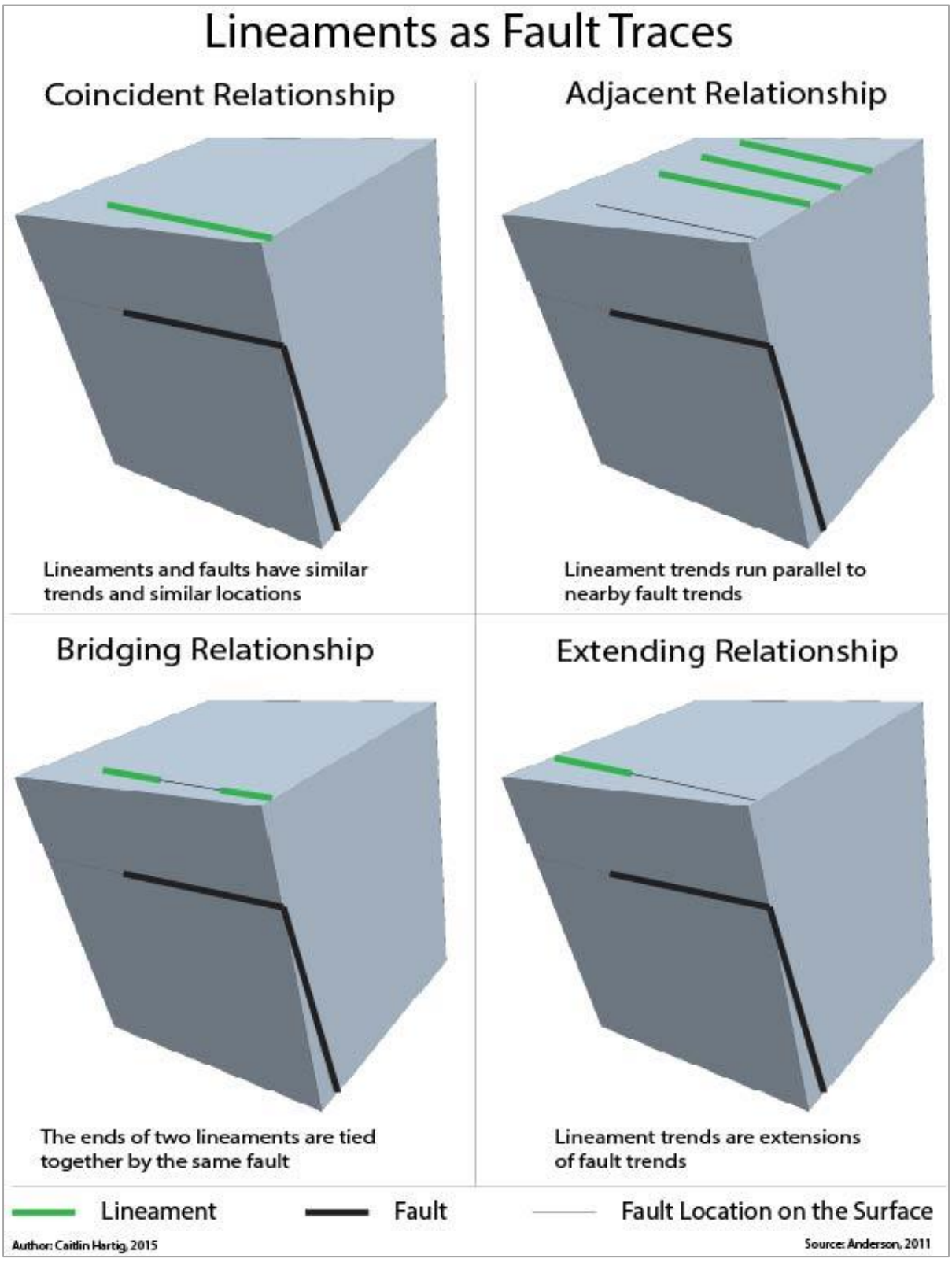

Figure 26: Lineaments as Fault Traces. Shows a coincident relationship, an adjacent relationship, a bridging relationship, and an extending relationship.

production wells for the SEGS should be placed northeast of the injection wells in order to maximize fluid flow.

DFN for Reservoir Simulation Modeling

More maps were made to show the locations of the basement faults and surface lineaments in the whole research area. Figure 27 shows the locations of known basement faults in the study area. Faults labeled "certain" have been identified based on both stratigraphic and seismic data, while faults labeled "probable" have only been identified from seismic data. Figure 28 shows the locations of all known surface lineaments in the study area and can be utilized, due to lack of better knowledge, as a proxy for the natural fractures in the subsurface. Figure 29 combines Figures 27 and 28 to show all known basement faults and all known surface lineaments in the study area; consequently, the shapefile displayed in Figure 29 can be utilized to represent the discrete fracture network (DFN) of the study area in a reservoir simulation model.

Furthermore, it has been shown that higher overall production rates correlate to areas of greater lineament density (Anderson, 2011). The greatest lineament density occurs in the northeastern corner of Williams County, which has 25 lineaments per 84.9 km^2 (0.94 lineaments/km^2) (Figure 30). Because the lineament density is greatest in the northeastern corner of Williams County, this part of the study area would be an ideal spot to test in a reservoir simulation model for placement of the SEGS.

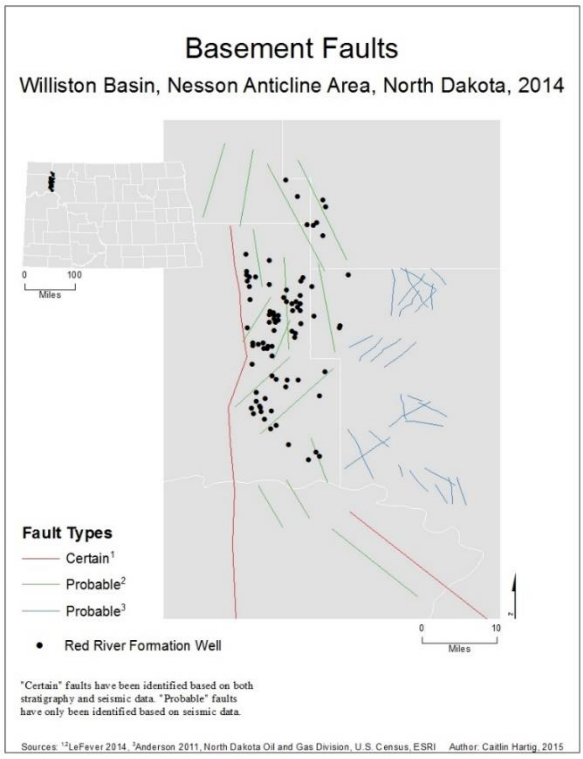

Figure 27: Basement Faults showcases known faults in or around the study area. "Certain" faults have been identified based on both stratigraphic and seismic data. "Probable" faults have only been identified based on seismic data.

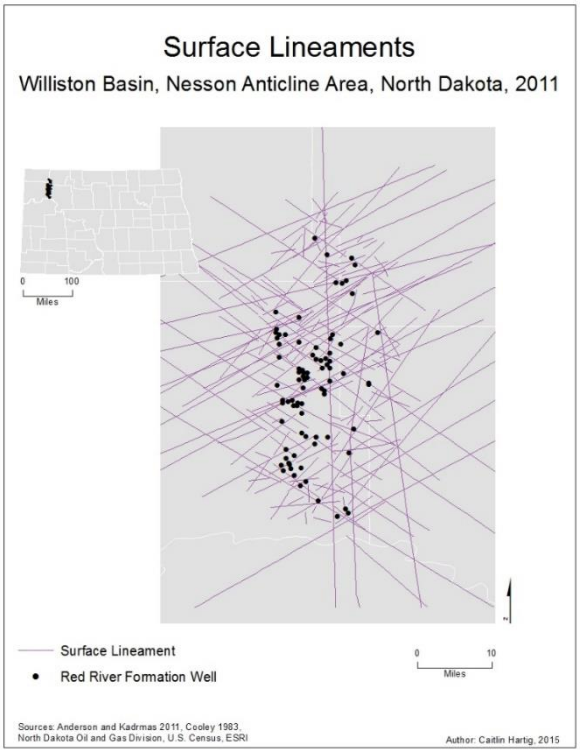

Figure 28: Surface Lineaments showcases known lineaments in the study area.

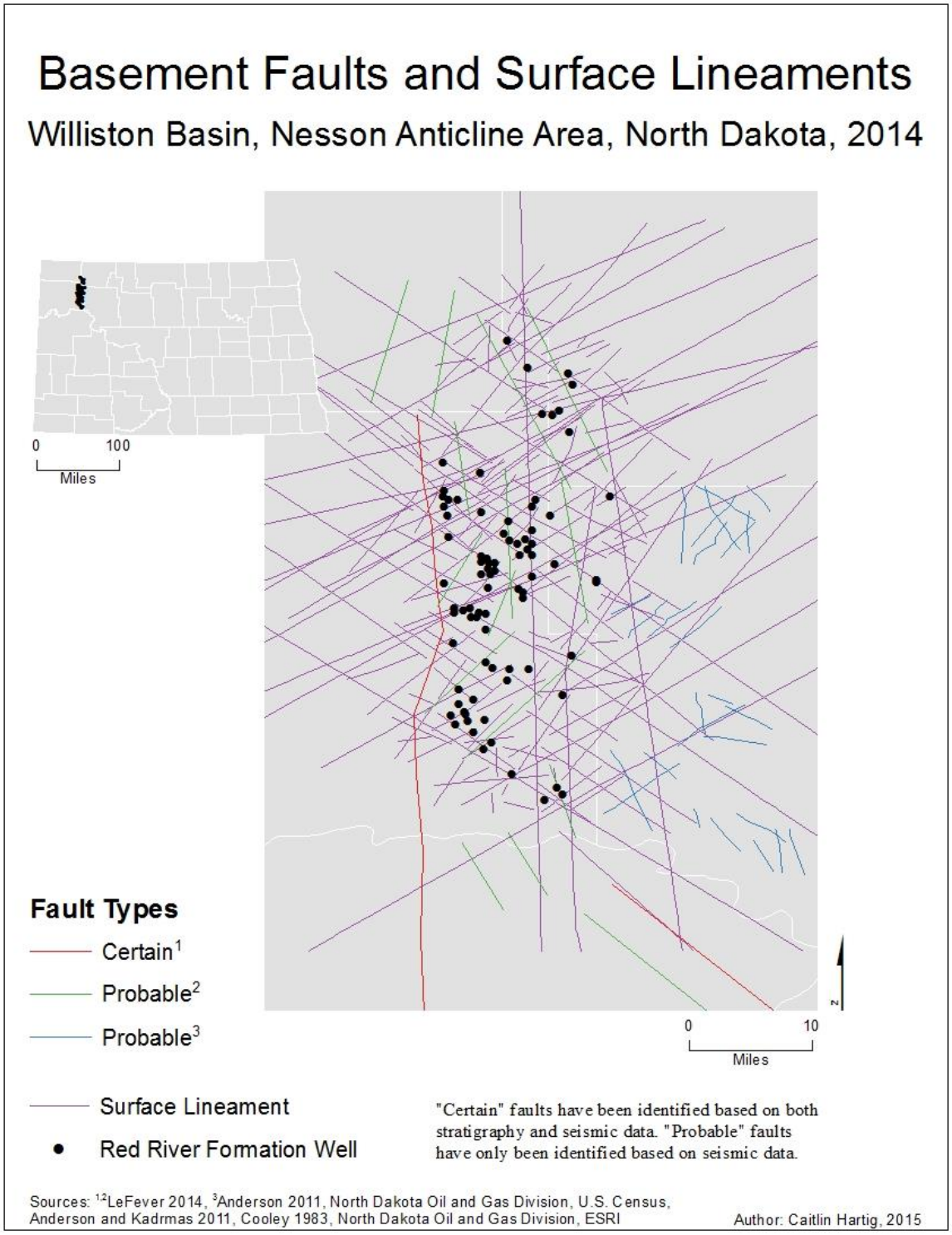

Figure 29: Basement Faults and Surface Lineaments in the study area. Because the surface lineaments and basement faults are spatially autocorrelated, it can be assumed that the surface lineaments mimic the trends of the natural fracture network in the subsurface. Therefore, the shapefile shown in this map can be utilized in reservoir simulation modeling to represent the discrete fracture network of the study area.

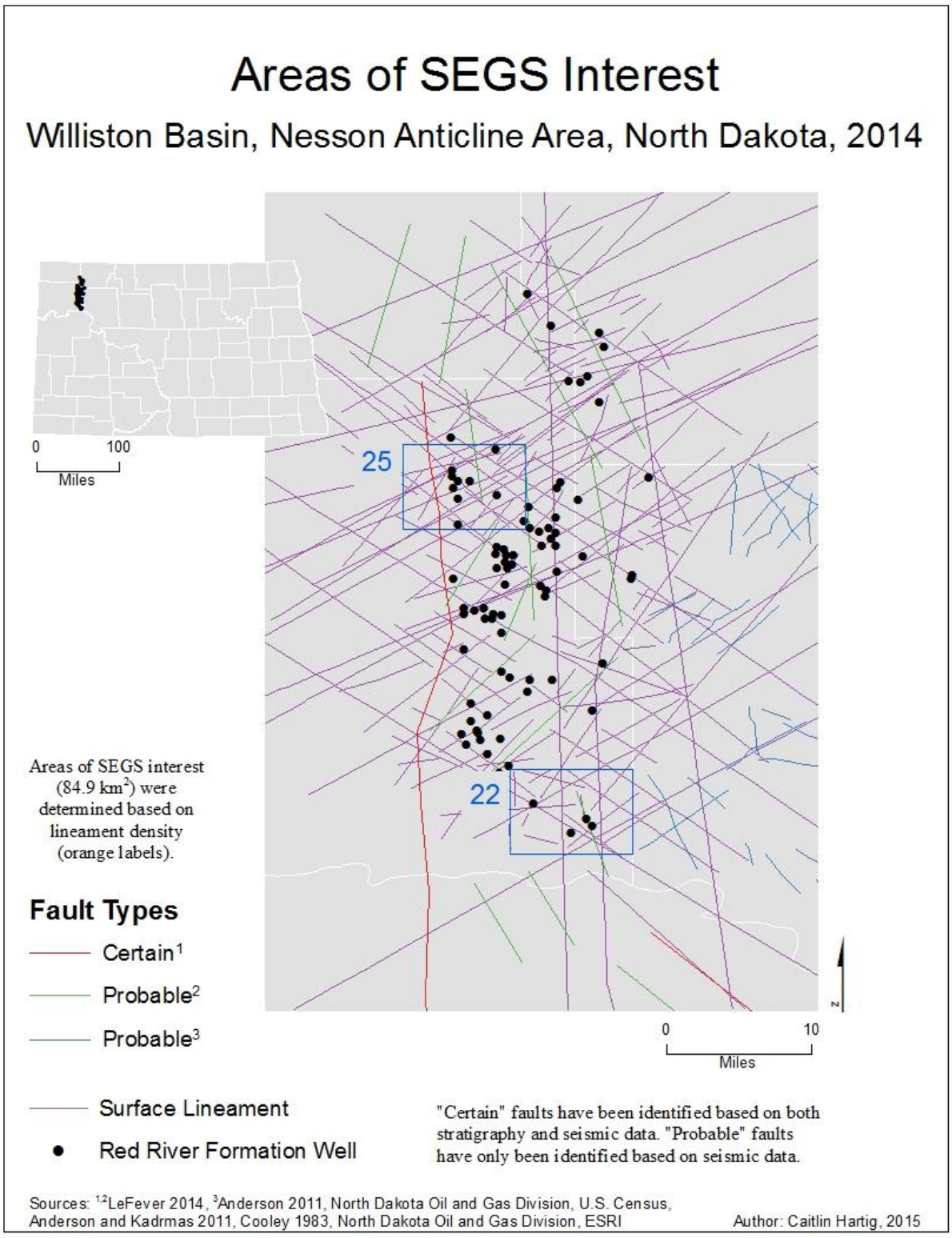

Figure 30: Areas of SEGS Interest are shown based on lineament density. Blue rectangles that are 9.016 km by 9.417 km (84.9 km²) highlight a section of northeastern Williams County with 25 lineaments and a section of southeastern Williams County with 22 lineaments.

CHAPTER IV

FUTURE RESEARCH

Reservoir Simulation Modeling Objectives

A reservoir simulation model will be completed in the future to continue this research. Chad Augustine and his team at NREL have begun the process of modeling the reservoir using Computer Modelling Group (CMG) STARS Advanced Processes Thermal Reservoir Simulator. The objectives of the reservoir simulation modeling will be 1) to describe the process of hydroshearing design, 2) to emphasize critical design factors that determine design effectiveness, and 3) to investigate the optimal treatment selection for an SEGS in the Red River Formation. Moreover, an economic analysis of the SEGS system will be conducted in order to evaluate the financial performance of different treatment scenarios.

Location of SEGS

The results of the GIS analyses can be input into a reservoir simulation model in order to ascertain the response of the Red River Formation to SEGS and fracture stimulation. The ideal location for an SEGS would be 1) where the temperature in the subsurface is the hottest, and 2) where there is high natural fracture density. Ideally, the hottest temperatures in the formation would need a medium of transport (natural fractures) to be conducive to good fluid flow and system mechanics. One location to test for the SEGS placement should be the south-central part of the study area (the southeastern part of Williams County) in order to tap the hottest temperatures in the Red River Formation within the research area (Figures 14 and 18). A second location to test for the SEGS placement would be the central part of the study

area (the northeastern corner of Williams County) in order to obtain the best production results from the greatest amount of lineaments (natural fractures) (Figure 30). While the southeastern part of Williams County has 22 lineaments (natural fractures) per 84.9 km^2 (0.259 lineaments/km^2), the northeastern corner of Williams County has 25 lineaments (natural fractures) per 84.9 km^2 (0.294 lineaments/km^2) (Figure 30). On the other hand, the northeastern corner of Williams County has temperatures ten degrees colder than the southeastern part of Williams County (Figures 14 and 18). Because the southeastern part of Williams County has the hottest temperatures in the study area in addition to a high natural fracture density, and because the northeastern corner of Williams County has the highest natural fracture density in addition to the second hottest temperatures in the study area, both areas should be investigated in the reservoir simulation model as potential sites for SEGS installation.

Modeling Deliverable

Ultimately, the reservoir simulation modeling will have the deliverables of a thermal recovery assessment of the sedimentary geothermal reservoir to be installed in the Red River Formation utilizing hydroshearing. The thermal recovery assessment will be complete with analysis of the fluid injection rate, amount, and pressure. Furthermore, the amount of spacing between the injection and production wells will be determined. A financial analysis of the thermal recovery assessment will be completed in order to determine whether an SEGS would be beneficial to install in the Red River Formation. It is predicted that the cost of the SEGS installation will be offset by high productivity from the reservoir.

CHAPTER V

CONCLUSION

Potential Obstacles

There are three potential obstacles to the realization of this project: 1) contamination of potable drinking water, 2) formation of gypsum scale, and 3) accumulation of sufficient water for SEGS operation. These problems are addressed below.

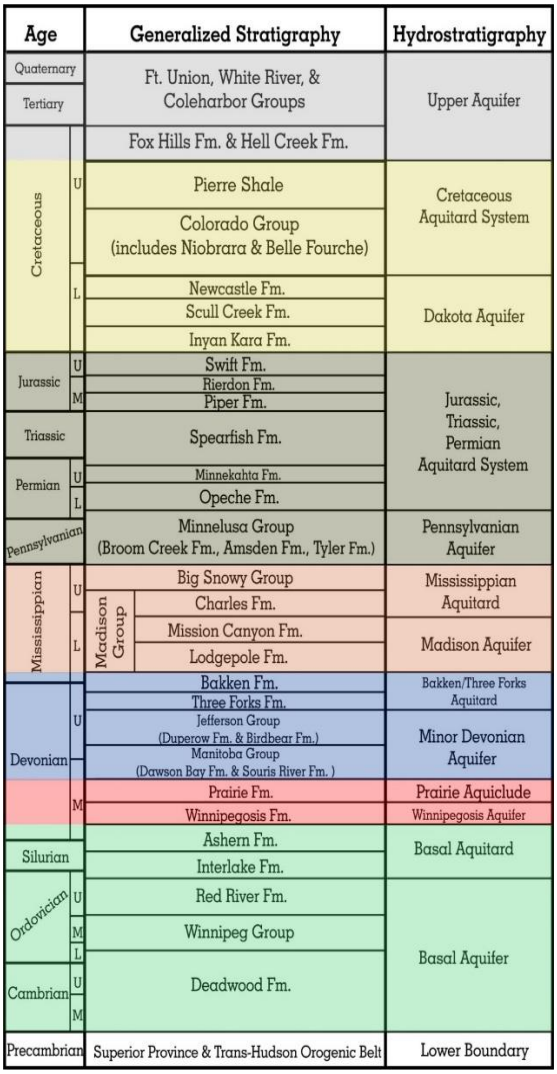

Figure 31: Hydrostratigraphy of the Williston Basin (Faye Ricker, Pers. Comm., 2015).

Whenever fluids are injected into the ground, a question is presented as to whether or not the project will result in the contamination of potable water. Currently, potable drinking water in the Williston Basin is pumped from the Fox Hills Formation in the Upper Aquifer (Whitehead, 1996). The Red River Formation, on the other hand, is located much deeper, in the basal aquifer (Figure 31). As a result of this, the Red River Formation is too deep to be utilized for drinking water. Furthermore, the Red River Formation water consists of saline brine with a total dissolved solid (TDS) concentration greater than 100,000

milligrams per liter (Whitehead, 1996). Therefore, even if water were to be extracted from Red River Formation, the water extracted from it would not be potable. Finally, SEGS fluids that would be injected into the Red River Formation could not contaminate the overlying aquifers because the Red River Formation is directly overlain by the basal aquitard (Figure 31).

The next potential problem of this project is that anhydrite ($CaSO_4$) traces are found in the Red River Formation limestones and dolostones. As a result of this, gypsum ($CaSO*2H_2O$) scale will accumulate and clog the formation when water is injected into the reservoir in the SEGS. Because there are only traces of anhydrite in the formation, it is unlikely that gypsum formation would be ubiquitous. Moreover, the gypsum formation process could be impeded by periodically diluting the reservoir with fresh water (Crabtree, 1999). In the event that gypsum scale were to accumulate in spite of periodic dilution, the scale could be removed with an acid treatment that contains a chelating agent, for instance ethylenediamenetetra-acetic acid (EDTA). The chelating agent is necessary because the sulfate scale is difficult to remove as a result of its low solubility in acid (Crabtree, 1999).

The final potential problem of this project is that many gallons of water are needed to continuously operate an SEGS. The reason for this is that 1) water needs to be injected continuously into the reservoir to extract heat, and 2) water needs to be injected periodically into the reservoir to complete the hydroshearing process. Consequently, the SEGS would need to be located near an abundant source of water. One possible water source is the Missouri River, which flows along the southern boundaries of Williams and Mountrail counties. Fortuitously, the southeastern part of Williams County, where temperatures in the study area are hottest, is only 1.3 miles away from the Missouri River. Given this

information, the SEGS site should be located in the southeastern part of Williams County, rather than in the northeastern corner of Williams County.

Revisiting the Hypothesis

Thus far, SEGS is feasible in the Red River Formation of the Williston Basin in western North Dakota. In the proposed SEGS site in the southeastern part of Williams County, temperature is sufficiently high (140° C) and porosity and permeability are high enough (17% and 0.1-38 mD, respectively) to yield a large volume of fluid. The presence of a DFN in the subsurface further facilitates flow.

Currently, there are no major problems that would impede the completion of a successful project. However, once the results of the reservoir simulation modeling are obtained, the hypothesis can either be fully supported or fully refuted with certainty.

Overall Project Benefits

This project will result in an overall improved knowledge of SEGS and of the existing geothermal potential in the Red River Formation of the Williston Basin in western North Dakota. This improved knowledge will consequently lower the drilling risk for the area. As a result of the reduced drilling risk, there will be lower drilling and completions costs. As a result of the lowered costs, the geothermal industry will flourish.

APPENDIX

APPENDIX A
List of Tables

Table 1. North Dakota Stratigraphic Column Maximum Thicknesses and NDGS Well 5086 TSTRAT

Formation	Maximum Thickness* (m)	Well 5086 Depth to Formation Top** (m)
Brule	61	382.5
Chadron	43	
Golden Valley	122	438.75
Tongue R.	396	487.5
Slope Fm.	82	
Cannonball Fm.	78	
Ludlow	91	
Hell Creek	101	937.5
Fox Hills	122	1087.5
Pierre	701	1177.5
Niobrara	76	1702.5
Carlisle	122	1758.75
Greenhorn	46	1848.75
Belle Fourche	107	1882.5
Mowry	91	1961.25
Newcastle	46	2002.5
Skull Creek	43	2036.25
Inyan Kara	191	2066.25
Swift	221	2227.5
Rierdon	30	2340
Piper	191	2362.5
Spearfish	229	2505
Minnekahta	21	2673.75
Opeche	152	2682.5
Broom Creek	114	2772.75
Amsden	137	2847.75
Tyler	82	2874
Otter	61	2934
Kibbey	76	2979
Charles	225	3035.25
Mission Canyon	303	
Lodgepole	225	
Bakken	49	3845.25
Three Forks	82	3511.5
Bird Bear	46	3567.75
Duperow	163	3597.75
Souris R.	114	3702.75

Table 1. cont.

Dawson Bay	58	3781.5
Prairie	198	3822.75
Winnepegosis	67	3972.75
Interlake	390	4062.75
Stonewall	37	4314
Stony Mountain	76	4340.25
Red River	213	4385.25
Winnipeg	161	4546.5
Deadwood	305	4640.25
PreCambrian	--	4740
Sum of Maximum Thicknesses:	**6545**	--

*Murphy et al., 2009
**NDGS Well 5086 TSTRAT

Table 2. Red River Formation Depth, Thickness, Permeability, and Porosity

Well	Depth to the Top of the Formation (km)	Depth to the Bottom of the Formation (km)	Thickness* (km)	Permeability** (mD)	Δt_{log}**	Porosity** (%)
32	3.91	4.09	0.180			
235	3.84	4.00	0.154			11
355	3.83	4.01	0.184			
1231	3.86	4.04	0.176			
1385	4.00	4.20	0.197	6.2		
1636	3.96	4.15	0.191			
2009	3.84	3.99	0.154			
3844	3.94	4.14	0.198		55	5
4321	3.88	4.06	0.184			4
4323	3.84	4.02	0.182			10
4340	4.07	4.22	0.154		50	2
4379	3.85	3.92	0.067	9.3	54	5
4390	3.85	4.00	0.154			25
4420	3.88	4.03	0.154		58	10
4434	3.88	4.03	0.154		55	5
4514	3.90	4.05	0.154			
4665	3.81	3.97	0.154		53	7
4716	3.88	4.07	0.189		54	5
5069	3.92	4.12	0.192			5
5192	3.64	3.79	0.154			8
5197	3.87	4.02	0.154			9
5545	3.86	4.02	0.154			

Table 2. cont.

5577	3.83	4.02	0.182			18
5612	3.86	4.02	0.154			19
5648	3.85	4.00	0.154			15
5656	3.87	4.02	0.154	0.5		15
5658	3.86	4.01	0.154			
5725	3.87	4.06	0.189			19
5726	3.85	4.00	0.154			18
5912	3.90	4.09	0.192			25
5937	3.87	4.06	0.188			20
6029	3.89	4.04	0.154			21
6087	3.91	4.06	0.154			18
6098	4.05	4.26	0.208			18
6108	3.86	4.01	0.154			18
6111	3.88	4.04	0.154			21
6362	3.92	4.08	0.154			17
6545	3.81	3.91	0.101			
6569	4.02	4.17	0.154			19
6915	4.12	4.21	0.090	0.1		11
7005	3.94	4.15	0.204			12
7557	3.87	4.03	0.154			20
7595	3.87	4.02	0.154			20
7856	3.80	3.96	0.154			
8645	3.98	4.02	0.046			20
8689	3.95	4.05	0.104			11
8722	3.83	3.91	0.076			13
9207	3.82	3.97	0.154			13
9361	3.85	4.00	0.154			14
9642	3.85	3.99	0.142			19
9801	3.86	4.01	0.154			15
10073	3.84	4.00	0.154			22
10328	3.84	4.00	0.154			13
11089	3.89	4.04	0.154	0.535		13
11126	3.86	4.01	0.154			11
11164	3.85	4.00	0.154			10
11405	3.84	4.00	0.154			15
11760	4.13	4.18	0.054			
12024	3.88	4.07	0.190			17
12035	3.76	3.92	0.154			16
12109	3.77	3.92	0.154			27
12119	3.83	4.00	0.173	1.08		10

Table 2. cont.

12261	3.74	3.90	0.154			14
12270	3.83	4.00	0.175	3		9
12290	3.80	3.95	0.154			14
12305	3.97	4.15	0.183			17
12329	3.75	3.90	0.154			15
12363	3.87	4.06	0.186			14
12366	3.78	3.93	0.154			14
12432	3.87	4.05	0.181			9
12556	3.93	4.08	0.154			22
12592	3.94	4.12	0.181			15
12597	3.91	4.10	0.191			14
12790	3.87	4.02	0.154	38		
12906	3.65	3.80	0.154			
12917	3.89	4.04	0.154			8
12971	4.00	4.20	0.197	19.9		23
13395	3.87	4.06	0.186	22.8		24
13682	3.91	4.09	0.184			12
15089	3.90	4.05	0.154			15
18680	3.93	4.14	0.204			

*Thickness of 0.154 km refers to the average unit thickness value for the Red River Formation as calculated from the maximum thickness of the Red River Formation from the NDGS North Dakota Stratigraphic Column (Murphy et al., 2009) correlated to NDGS Well 5086 (in essence, the value from Murphy et al., 2009 corrected by a factor of 0.72). The thickness of 0.154 km was utilized to calculate the depth to the bottom of the formation for wells in which that depth was unavailable from the North Dakota Oil and Gas Division website.
**Measurements were obtained only for Red River Unit C.

Table 3. NDGS Well 6840: Temperature, Thermal Conductivity, Depth, Thickness, and HMC

Formation	**Temperature (°C)**	**λ (W/mK)**	**Depth (m)**	**Thickness (m)**	**Harmonic Mean Conductivity (K/W)**
Brule	6	1.2	49	49.41	41.18
Chadron	6	1	84	34.83	34.83
Golden Valley	6	1.4	183	98.82	70.59
Tongue R.	14.8	1.3	433	250	192.3
Slope	17.3	1.3	499	66.42	51.09
Hell Creek	20.3	1.3	581	81.81	62.93
Fox Hills	24.1	1.2	680	98.82	82.35
Pierre	47.2	1.2	1248	567.81	473.2
Niobrara	49.8	1.1	1309	61.56	55.96
Carlisle	54.2	1.2	1408	98.82	82.35
Greenhorn	54.8	1.1	1423	14.7	13.36
Belle Fourche	57.5	1.1	1484	61	55.45
Mowry	60.6	1.1	1555	71	64.55
Newcastle	62.6	1.5	1599	44	29.33

Table 3. cont.

Skull Creek	63.6	1.3	1630	31	23.85
Inyan Kara	65.3	1.6	1676	46	28.75
Swift	69.6	1.2	1816	140	116.7
Rierdon	75.6	1.6	1963	147	91.88
Piper	77.2	1.6	2015	52	32.5
Spearfish	81.3	1.6	2149	134	83.75
Minnekahta	85.5	2.5	2285	136	54.4
Opeche	85.7	1.2	2294	9	7.5
Broom Creek	88.5	2.2	2363	69	31.36
Amsden	90.0	4.0	2432	69	17.25
Tyler	90.3	1.2	2455	23	19.17
Otter	92.7	1.2	2514	59	49.17
Kibbey	94.3	2.7	2553	39	14.44
Charles	95.4	2.5	2614	61	24.5
Mission Canyon	97.2	2.5	2705	91	36.55
Lodgepole	100.9	2.5	2892	187	75.1
Bakken	104.5	1.1	3073	181	164.5
Three Forks	105.6	3.1	3098	25	8.065
Bird Bear	106.4	3.1	3152	54	17.25
Duperow	106.9	3.2	3181	29	9.091
Souris R.	108.4	2.9	3282	101	34.59
Dawson Bay	109.7	2.8	3358	76	27.64
Prairie	110.4	4.0	3397	39	9.75
Winnepegosis	112.2	3.0	3542	145	48.49
Interlake	113.5	3.8	3621	79	20.95
Stonewall	116.6	3.9	3863	242	62.21
Stony Mountain	116.9	3.8	3888	25	6.596
Red River	117.5	3.3	3932	44	13.41
Winnipeg	119.8	4.1	4087	155	38.08
Deadwood	120.9	3.5	4177	90	26.01
PreCambrian	61.7	2.6	4482	217	--

Table 4. Red River Formation BHTs, Geothermal Gradient, Heat Flow, and Predicted Temperatures

Well	**BHT (°C)**	**Harrison Correction (°C)**	**Corrected BHT (°C)**	**Geothermal Gradient* (°C/km)**	**λ_{basin} (W/mK)**	**Heat Flow** (mW/m^2)**	**Predicted Temperature (°C)**
32						55.00	144
235	110	19	129	32.08	1.667	53.47	138
355						55.00	142
1231						55.00	143

Table 4. cont.

1385						55.00	148
1636						55.00	146
2009						57.00	147
3844						55.00	145
4321						55.00	143
4323						55.00	142
4340	130	19	149	35.19	1.667	58.67	149
4379						55.00	142
4390	113	19	132	32.74	1.667	54.58	141
4420	118	19	137	33.81	1.667	56.36	146
4434	117	19	136	33.50	1.667	55.85	145
4514	116	19	135	33.19	1.667	55.32	145
4665	122	19	141	35.54	1.667	59.25	151
4716						55.00	143
5069						55.00	145
5192	110	19	129	33.81	1.667	56.37	138
5197	110	19	129	31.88	1.667	53.14	138
5545						55.00	143
5577						55.00	142
5612	126	19	145	35.95	1.667	59.92	155
5648	113	19	132	32.76	1.667	54.61	141
5656	113	19	133	32.74	1.667	54.58	142
5658						55.00	143
5725						55.00	143
5726	112	19	131	32.61	1.667	54.35	141
5912						55.00	144
5937						55.00	143
6029	110	19	129	31.72	1.667	52.88	138
6087	109	19	128	31.27	1.667	52.13	137
6098						57.00	154
6108	113	19	133	32.80	1.667	54.68	142
6111	119	19	139	34.17	1.667	56.96	148
6362	119	19	139	33.81	1.667	56.37	148
6545						57.00	146
6569	104	19	124	29.30	1.667	48.85	133
6915	118	19	137	31.90	1.667	53.18	147
7005						57.00	150
7557	121	19	140	34.56	1.667	57.61	149
7595	113	19	132	32.57	1.667	54.29	141
7856						57.00	145

Table 4. cont.

8645	106	19	125	29.87	1.667	49.79	134
8689	111	19	130	31.50	1.667	52.51	140
8722	121	19	140	35.08	1.667	58.48	150
9207	117	19	136	34.03	1.667	56.73	145
9361	112	19	131	32.45	1.667	54.10	140
9642	124	19	144	35.76	1.667	59.61	153
9801	112	19	131	32.51	1.667	54.19	141
10073	124	19	144	35.83	1.667	59.73	153
10328	109	19	128	31.78	1.667	52.98	137
11089	127	19	146	36.14	1.667	60.24	156
11126	109	19	128	31.64	1.667	52.74	137
11164	105	19	124	30.76	1.667	51.27	133
11405	128	19	147	36.69	1.667	61.15	157
11760	132	19	151	35.24	1.667	58.74	161
12024						55.00	144
12035	118	19	138	34.97	1.667	58.29	147
12109	118	19	137	34.78	1.667	57.98	146
12119						57.00	146
12261	114	19	134	34.12	1.667	56.87	143
12270	125	19	144	36.11	1.667	60.20	154
12290	118	19	137	34.49	1.667	57.49	146
12305	121	19	140	33.88	1.667	56.47	143
12329	112	19	131	33.47	1.667	55.79	141
12363						55.00	143
12366	114	19	134	33.81	1.667	56.36	143
12432						55.00	143
12556	116	19	135	32.80	1.667	54.68	144
12592						55.00	145
12597	127	19	146	35.77	1.667	59.62	156
12790	117	19	136	33.59	1.667	56.00	145
12906	114	19	133	34.80	1.667	58.02	142
12917	118	19	137	33.72	1.667	56.21	146
12971						55.00	148
13395						55.00	143
13682						55.00	144
15089	118	19	138	33.74	1.667	56.25	147
18680						55.00	145

*Geothermal gradient was calculated by subtracting a surface temperature of 6° C from the corrected BHT and dividing that value by the depth to the top of the formation in km listed in Table 1.
**Heat flow for wells without BHT measurements was predicted from well placement in Figure 13.

REFERENCES

Anderson, Fred J., 2008, Lineament mapping and analysis in the northeastern Williston Basin of North Dakota: North Dakota Geological Survey, Geological Investigations No. 70, p. 26.

Anderson, Fred J., 2011, Structural Relationships between Surface Lineaments and Basement Faulting in the Northeastern Williston Basin: The Rocky Mountain Association of Geologists (RMAG), p. 376-392.

Anderson, Fred J., and Kadrmas, Elroy, compilers, 2011, Shapefile of historic surface lineaments in the Williston 250k.

Anderson, Tom C., 2013, Geothermal Potential of Deep Sedimentary Basins in the United States, *in* GRC Transactions, A Global Resource, from Larderello to Las Vegas, Volume 37: Davis, CA, Geothermal Resources Council, p. 223-229.

Bell, J.S., and Grasby, S.E., 2012, The stress regime of the Western Canadian Sedimentary Basin, *in* Geofluids, Volume 12: p. 150-165.

Blackwell, David D., et al., 2006, Geothermal Resources in Sedimentary Basins: Southern Methodist University.

Blackwell, D.D., and Richards, M., 2004a, Geothermal Map of North America Explanation of Resources and Applications: Southern Methodist University.

Blackwell, D.D., and Richards, M., 2004b, Geothermal Map of North America: AAPG, scale 1:6,500,000, Product Code 423.

Blodgett, Leslie, 2010, Developing Geothermal Energy at Low Temps: http://www.renewableenergyworld.com/rea/news/article/2010/09/low-t (accessed February 2014).

Chabora, Ethan, and Zemach, Ezra, 2013, Desert Peak EGS Project: U.S. Department of Energy.

Chen, Zhuoheng, et al., 2009, Spatial variation of Bakken or Lodgepole oils in the Canadian Williston Basin, *in* AAPG Bulletin, Volume 93, number 6: p. 829-851.

Chen, Zhuoheng, et al., 2011, Geologic controls on regional transmissivity anisotropy, *in* Geofluids, Volume 11: p. 228-241.

Cooley, M. E., 1983, Linear features determined from LANDSAT imagery in North Dakota: USGS Open File Report 83-937.

Crabtree, Mike, et al., 1999, Fighting Scale—Removal and Prevention: Oilfield Review, p. 30-45.

Crowell, Anna M., et al., 2011, GIS Analysis for the Volumes, and Available Energy of Selected Reservoirs: Williston Basin, North Dakota., *in* GRC Transactions, A Global Resource, from Larderello to Las Vegas, Volume 35: Davis, CA, Geothermal Resources Council, p. 1581-1585.

Crowell, Anna M., and Gosnold, W.D., Jr., 2011, Correcting Bottom-Hole Temperatures: A Look at the Permian Basin (Texas), Anadarko and Arkoma Basins (Oklahoma), and Williston Basin (North Dakota), *in* GRC Transactions, A Global Resource, from Larderello to Las Vegas, Volume 35: Davis, CA, Geothermal Resources Council, p. 735-738.

Freisatz, Wayne B., 1991, Fracture-enhanced Porosity and Permeability Trends in the Bakken Formation, Williston Basin, Western North Dakota [Master's thesis]: University of North Dakota.

Freisatz, Wayne B., 1995, Fracture-enhanced Porosity and Permeability Trends in the Bakken Formation, Williston Basin, Western North Dakota: Proceedings of Seventh International Williston Basin Symposium.

Geothermal energy Hot rocks, 2014, *in* The Economist, p. 54-55.

Gerhard, L.C., et al., 1987, Structural History of the Nesson Anticline, North Dakota, *in* Williston Basin: Anatomy of a Cratonic Oil Province, p. 337-354.

Gerhard, L.C., et al., 1990, Petroleum geology of the Williston Basin, *in* M.W. Leighton, D.R. Kolata, D.F. Oltz, and J.J. Eidel, eds., Interior cratonic basins: AAPG Memoir, Volume 51: p. 509-559.

Gosnold, W.D., Jr., 1984, Geothermal Resources in the Williston Basin: North Dakota, *in* GRC Transactions, A Global Resource, from Larderello to Las Vegas, Volume 8: p. 431-436.

Gosnold, W.D., Jr., 1991, Subsurface temperatures in the northern Great Plains, *in* Slemmons, D.B., Engdahl, E. R., Zoback, M.D., and Blackwell, D.D., eds., Neotectonics of North America: Boulder, Colorado, Geological Society of America, Decade Map Volume I: p. 467-472.

Gosnold, W.D., Jr., 1999, Basin-Scale groundwater flow and advective heat flow: An example from the northern Great Plains, *in* Forster and Merriam, eds., Geothermics in Basin Analysis: Kluwer Academic/Plenum, p. 99-116.

Gosnold, W.D., Jr., et al., 2010, EGS Potential in the Northern Midcontinent of North America, *in* GRC Transactions, A Global Resource, from Larderello to Las Vegas, Volume 34: Davis, CA, Geothermal Resources Council.

Gosnold, W.D., Jr., et al., 2012, Thermostratigraphy of the Williston Basin, *in* GRC Transactions, A Global Resource, from Larderello to Las Vegas, Volume 36: Davis, CA, Geothermal Resources Council.

Laird, W. M., and Folsom, C. B., Jr., 1956, North Dakota's Nesson anticline: North Dakota Geological Survey Report of Investigation 22, 12 p.

LeFever, Julie A., et al., 1987, Structural evolution of the central and southern portions of the Nesson Anticline, North Dakota: Proceedings of Fifth International Williston Basin Symposium, p. 147-156.

LeFever, Richard, 2014, Shapefile of basement faults in the Williston Basin, Nesson Anticline Area.

Morgan, Paul, 2013, Advantages of Choosing a Sedimentary Basin as the Site for an EGS Field Laboratory, *in* GRC Transactions, A Global Resource, from Larderello to Las Vegas, Volume 37: Davis, CA, Geothermal Resources Council, p. 179-183.

Murphy et al., 2009, North Dakota Stratigraphic Column: North Dakota Geological Survey: https://www.dmr.nd.gov/ndgs/documents/Publication_List/pdf/Strat-column-NDGS-%282009%29.pdf (accessed December 2014).

Penner, Lynden, 2006, Evidence Linking Surface Lineaments, Deep-Seated Faults, and Fracture-Controlled Fluid Movement in the Williston Basin: Proceedings of 14th Williston Basin Petroleum Conference & Prospect Expo.

Porro, Colleen, and Augustine, Chad, 2014, Estimate of Geothermal Energy Resource in Major U.S. Sedimentary Basins, Golden, Colorado, NREL.

Tanguay, Lillian Hess, and Friedman, Gerald M., 2001, Petrophysical Facies of the Ordovician Red River Formation, Williston Basin, USA: Carbonates and Evaporites, v. 16, no. 1, p. 71-92.

Tester, J.W., et al., 2006, The future of geothermal energy: Impact of enhanced geothermal systems (EGS) on the United States in the 21st century: Massachusetts Institute of Technology: http://mitei.mit.edu/publications/reports-studies/future-geothermal-energy (Accessed February 2014).

United States Census, 2014, TIGER/Line Shapefiles: http://www.census.gov/cgi-bin/geo/shapefiles2010/file-download (accessed September 2014).

Wegelin, A., 1987, Reservoir characteristics of the Weyburn field, southeastern Saskatchewan: Journal of Canadian Petroleum Technology, Volume 26: p. 60-66.

Whitehead, R.L., 1996, Ground Water Atlas of the United States, Segment 8: Montana, North Dakota, South Dakota, Wyoming: U.S. Geological Survey, p. I-2-I-24.

Wyllie, M.R.J., et al., 1958, An experimental investigation of the factors affecting elastic wave velocities in porous media: Geophysics, Volume 23: p. 459-493.

Zoback, Mark D, and Zoback, Mary Lou, 1991, Tectonic stress field of North America and relative plate motions, *in* Slemmons, D.B., Engdahl, E.R., Zoback, M.D., and Blackwell, D.D., eds., Neotectonics of North America: Boulder, Colorado, Geological Society of America, Decade Map Volume I: p. 339-366.

Zoback, Mary Lou, and Zoback, Mark D, 1989, Tectonic stress field of the continental United States, *in* Pakiser, L.C., and Mooney, W.D., Geophysical framework of the continental United States: Boulder, Colorado, Geological Society of America, Memoir 172, p. 523-539.

Zoback, M.L., 1989, State of Stress and Modern Deformation of the Northern Basin and Range Province: Journal of Geophysical Research, Volume 94, number B6: p. 7105-7128.

Zoback, M.D., et al., 1985, Well Bore Breakouts and in Situ Stress: Journal of Geophysical Research, Volume 90, number B7: p. 5523-5530.